**Tissue-mimicking gelatin scaffolds by alginate sacrificial templates for adipose tissue engineering**

**Authors** Nicola Contessi Negrini[¥,†,§], Mathilde Bonnetier[¥], Giorgio Giatsidis[‡], Dennis P Orgill[‡], Silvia Farè[†,§,*], Benedetto Marelli[¥,*]

**Affiliations**

[¥]Department of Civil and Environmental Engineering, Massachusetts Institute of Technology, 77 Massachusetts Ave, Cambridge, MA, United States

[†]Department of Chemistry, Materials and Chemical Engineering "G. Natta", Politecnico di Milano, Piazza Leonardo da Vinci 32, 20133 Milan, Italy

[§]INSTM, National Interuniversity Consortium of Materials Science and Technology, Local Unit Politecnico di Milano, Piazza Leonardo da Vinci 32, 20133 Milan, Italy

[‡]Division of Plastic Surgery, Brigham and Women's Hospital, 75 Francis Street, Boston, MA, United States

*Correspondence should be addressed to: • Benedetto Marelli bmarelli@mit.edu

• Silvia Farè silvia.fare@polimi.it

**Abstract**

When adipose tissue (AT) is impaired by trauma or disease, AT engineering could provide a shelf-ready structural and functional restoration as alternative to current clinical treatments, which mainly aim at aesthetic replacement. Yet, the lack of an efficient vascular network within the scaffolds represents a major limitation to their translation application in patients. Here, we propose the use of microstructured crosslinked gelatin hydrogels with an embedded prevascular channel as scaffolding materials for AT engineering. The scaffolds are fabricated using – simultaneously – alginate-based microbeads and 3D printed filaments as sacrificial material encapsulated in gelatin at the point of material fabrication and removed post-crosslinking. This method yields the formation of microstructures that resemble the micro-architecture of physiological human fat tissue and of microvessels that can facilitate vascularization through anastomosis with patients' own blood vessels. The cytocompatible method used to prepare the gelatin scaffolds showed structural stability over time while allowing for cell infiltration and protease-based remodeling/degradation. Scaffolds' mechanical properties were also designed to mimic the one of natural breast adipose tissue, a key parameter for AT regeneration. Scaffold's embedded channel (∅ = 300 – 400 μm) allowed for cell infiltration and enabled blood flow *in vitro* when an anastomosis with a rat blood artery was performed using fibrin glue. *In vitro* tests with human mesenchymal stem cells (hMSC) showed colonization of the porous structure of the gelatin hydrogels, differentiation into adipocytes and accumulation of lipid droplets, as shown by Oil Red O staining.

**Keywords**

Gelatin, hydrogel; adipose tissue engineering; alginate; vascularization; 3D printing; sacrificial materials.

## 1. Introduction

The resection of tumors (e.g., breast cancer) and the treatment of traumatic injuries often requires the restoration of adipose tissue (AT), given its functional, aesthetic [1] and psychological [2] roles in patient well-being. Current clinical approaches only target the aesthetic reconstruction of the lost AT volume [3]; fillers are injected for small volumes (i.e., 1 – 2 $cm^3$) reconstructions, while implants are used to treat larger volumes (i.e., volume > 200 $cm^3$) [4]. Nonetheless, fillers may cause inflammation, shape distortion, and need for repeated administration, with associated high costs [5], while synthetic prostheses (e.g., silicone breast implants) may lead to capsular contraction, changes in shape and/or rupture [6] – up to 15% incidence rate [7]. Autologous tissue transfer is also used in clinical procedures, but it is affected by donor site morbidity, fat necrosis (0 – 10% rate) and flap failure (up to 2% rate) [8]; moreover, initial survival of fat grafting is strictly connected to an appropriate oxygen diffusion, only possible in presence of an appropriate graft vascularization [9].

To address the clinical need for the restoration of functional AT, several biomaterials – from both synthetic [10–15] and natural [16–22] origin – have been coupled with cells from different sources [23] to simultaneously target aesthetic and functional AT regain. The following are well-established general consensus principles that guide the design of scaffolds for AT engineering [4]: (*i*) a porous structure (pores diameter > 100 μm), able to simultaneously mimic the microarchitecture of the native AT, allow cells infiltration and tissue ingrowth [24] and guarantee nutrients exchange [15,25,26]; (*ii*) adequate biochemical cues to promote and/or guide the cell-biomaterial interactions (e.g., cell adhesive motifs); (*iii*) mechanical properties tuned to mimic mechanical response of native AT, matching, for example, subcutaneous AT elastic modulus (2 – 4 kPa) [27], and provide structural integrity with adjacent tissues and a biomimetic niche for AT stem cells; (*iv*) degradability and degradation rate that can support native AT regeneration; (*v*) promoted vascularization, either by vasculogenesis or angiogenesis [28], to address critical sized defects. In particular, the lack of an embedded vascular system has hindered the fabrication of engineered AT with clinical relevant dimensions [29]. Diffusion of oxygen, nutrients, metabolites and catabolites has in fact limited the dimension of cellularized scaffolds to less than few millimeters in thickness [30].

Despite the progresses made in the production and fabrication of scaffolds for AT engineering, matching all the AT scaffold requirements is still an open challenge. Several solutions have been proposed so far to

successfully achieve the (*i* – *iv*) requirements, while vascularization (*v*) still remains a critical issue to be addressed, especially when engineering substitutes for AT, a highly vascularized tissue where the adipogenic process is strictly connected to the formation of an efficient vasculature in the tissue [31]. Recently, indirect 3D printing technologies (i.e., sacrificial 3D printed structures embedded in the scaffold and subsequently removed) have emerged as alternative (or complementary) methods to promote vasculogenesis in engineered tissues [32–38]. Criteria for the selection of materials to be used in sacrificial templates include: rheological properties compatible with the requirements of 3D printing technologies, mechanical properties that are sufficient to maintain shape and geometry of the printed material during the scaffold handling and preparation, and ease of material removal in non-harsh conditions and with no cytotoxic side-effects to form hollow channels that would eventually promote vascularization. Although different materials and removal strategies have been tested for the production of sacrificial vascular networks, including gelatin [32,33], carbohydrate glass [34], agarose [35], alginate [36], Pluronic F127 [37], poly(N-isopropylacrylamide) (PNIPAM) [39] and PVA [38], none of these strategies has been proposed, to date, for the production of AT scaffolds.

This study aims at producing a prevascular channel in tissue-mimicking crosslinked gelatin hydrogels for AT engineering. We propose here an integrated approach in which sacrificial alginate templates were used to simultaneously obtain a porous gelatin hydrogel – by sacrificial removal of alginate microbeads – and a hollow channel via sacrificial removal of 3D printed alginate hydrogel filaments. The successful fabrication of a hollow channel in gelatin hydrogels that mimic native AT in terms of porosity and compressive mechanical properties is demonstrated, together with studies of enzymatic degradation using collagenase type I. Additionally, *in vitro* tests using human mesenchymal stem cells showed that the scaffold promoted cell infiltration in the prevascular channel together with the support of cell proliferation and adipogenic differentiation.

## 2. Materials and Methods

All reagents were purchased from Sigma Aldrich, unless differently specified.

### 2.1. Chemically crosslinked gelatin hydrogels synthesis

A chemically crosslinked gelatin hydrogel was used as material for the production of scaffolds for AT engineering; the synthesis procedure was explained in detail elsewhere [40–42]. Briefly, gelatin powder (type A from porcine skin, 300 g Bloom) was dissolved in distilled water under stirring at 50 °C to obtain a 15% w/v gelatin solution. After gelatin complete dissolution, 80 µL of triethylamine (TEA) were added for 10 min to increase the solution pH above 10. After that, 23.3 mg of *N-N'*-methylenebis(acrylamide), MBA, used as crosslinker, were added to the gelatin solution and stirred for other 10 min; finally, the mixture was poured in a glass Petri dish (diameter Ø = 6 cm) and cured at 37 °C for 24 h to complete the crosslinking reaction.

### 2.2. 3D printing of sacrificial alginate hydrogel filaments

To obtain a channel in the crosslinked gelatin hydrogel, a 3D printed alginate hydrogel filament, obtained by $Ca^{2+}$ divalent ions crosslinking, is embedded in the gelatin hydrogel and, after complete gelatin crosslinking, selectively dissolved by $Ca^{2+}$ ions chelation to obtain a hollow vascularizable channel inside the hydrogel. In detail, first, alginate printing parameters were optimized; then, the optimal/quicker alginate hydrogel dissolution procedure was identified and, finally, the alginate filament is printed using optimized parameters, embedded in the gelatin hydrogel, and dissolved to obtain a hollow channel with the desired geometry (see section 2.4).

*Optimization of alginate printing parameters*

The solution used as ink for the 3D printing was prepared by dissolving 1 g of alginic acid sodium salt (from Brown Algae, low viscosity) in 10 mL of phosphate buffered saline (PBS) under stirring at room temperature (R.T.) overnight. For the printing, the .stl files containing the design to be printed were obtained using Rhinoceros software (version 5.0.2, Robert McNeel & Associates) and subsequently processed by Slic3r software (version 1.2.9) to obtain the final .gcode files. The 10% w/v alginate solution was loaded in the printing cartridge of a pneumatic 3D printer (Inkredible, CELLINK®) and dispensed by applying a 20 kPa pressure (i.e., lower pressure allowing alginate solution continuous flow from the syringe). After the printing, alginate was crosslinked by pipetting a 100 mM $CaCl_2$ solution on the printed filament, allowed to crosslink for 5 min. The printing parameters were optimized by investigating the deposited alginate filament dimension by varying the needle dimension (*i.e.*, 20, 21, 22 and 23 G) and the printing speed (*i.e.*, 1, 5 and

10 mm $s^{-1}$), both before and after alginate crosslinking (n = 3 measurements on n = 4 images per tested condition). The layer thickness was designed as 85% of the inner diameter of the mounted needle.

*Optimization of the 3D printed alginate hydrogel dissolution*

To optimize the alginate hydrogels dissolution procedure, alginate disks (n = 3, Ø = 2 cm, infill = 100%) were printed, weighted ($w_0$) and immersed in distilled water, 50 mM NaCl solution or 50 mM trisodium citrate solution. At established time points (*i.e.*, 5, 10, 15 and 20 min) samples were removed from the solution and weighted ($w_t$). The residual weight (RW%) of the samples was calculated according to (1):

$$RW\% = \frac{W_t}{W_0} \times 100 \qquad (1)$$

## 2.3. Preparation of sacrificial alginate hydrogel microbeads

The porosity in the gelatin hydrogel is obtained by adding alginate microbeads, used as sacrificial templates, during the gelatin hydrogels preparation. First, the alginate hydrogel microbeads production process was optimized to obtain microbeads with controlled and desired dimension; then, the quicker dissolution procedure was investigated and, finally, microbeads are embedded in the gelatin hydrogels to obtain a microporous structure (see section 2.4).

*Alginate microbeads production and dimensional distribution*

Alginate microbeads were produced by dropping a 2% w/v alginic acid sodium salt (from Brown Algae, low viscosity) in a 100 mM $CaCl_2$ solution under stirring (600 rpm). The microbeads production setup was composed by a syringe pump vertically mounted above a Beaker containing a 100 mM $CaCl_2$ solution; the distance between the needle and the $CaCl_2$ solution was set at 3.5 cm. The alginate solution was dropped at a rate of 15 mL $h^{-1}$ by an internal needle ($Ø_{int}$ = 0.4 mm) coaxially mounted with an external needle ($Ø_{int}$ = 0.7 mm) with an applied air flow (Figure 1C.*i*). Alginate microbeads (n = 400) were collected after the production process and their dimension analyzed by ImageJ software, reporting the diameter distribution in 20 µm intervals.

*Optimization of the alginate hydrogel microbeads dissolution*

Alginate microbeads were collected in Cell Strainer filters ($Ø_{pores}$ = 40 µm) and the microbeads dissolution was investigated by immersion in distilled water, 50 mM NaCl solution and 50 mM trisodium citrate (n = 3 per tested solution), as performed for the 3D printed alginate dissolution study to obtain RW% values (see section 2.2).

2.4. Vascularizable microporous gelatin hydrogel scaffolds

Microporous vascularizable gelatin hydrogel scaffolds were obtained by using gelatin loaded with alginate hydrogel microbeads (Figure 1A.*i*). Briefly, 1 g of alginate hydrogel microbeads were added per mL of gelatin solution, 10 min after the addition of MBA to the solution, and the gelatin solution containing the alginate microbeads was poured in a Petri dish (Ø = 6 cm). Then, a single, continuous alginate filament was designed with a "snake-like" structure and 3D printed on the crosslinked gelatin hydrogel (20 kPa, 21 G, 1 mm $s^{-1}$, Figure 1A.*ii*), crosslinked by 100 mM $CaCl_2$ solution for 5 min and, finally, 5 mL of gelatin containing alginate microbeads (1 g of microbeads per mL of gelatin solution) were poured on the crosslinked gelatin/alginate structure (Figure 1A.*iii*) and allowed to crosslink for 24 h at 37 °C. The obtained scaffolds (Figure 1A.*iv*) were immersed in 50 mM trisodium citrate solution for 24 h, sonicated for 30 min and washed with distilled water to simultaneously dissolve alginate microbeads, to obtain a microporous structure, and 3D printed alginate, after flushing trisodium citrate to obtain hollow a vascularizable channel (Figure 1A.*v*).

Similarly, GEL_bulk hydrogels were used to obtain non-microporous scaffolds, as control. 5 mL of gelatin solution (after the mixing of TEA and MBA) were poured in a glass Petri dish (Ø = 6 cm). Then, the obtained gelatin hydrogel layer was used as substrate for alginate printing (20 kPa, 21 G, 10 mm $s^{-1}$) and a $CaCl_2$ solution was poured on the printed filament to crosslink the alginate. Then, 5 mL of gelatin solution (after the mixing of TEA and MBA) were poured on the alginate printed on the crosslinked gelatin layer and the gelatin crosslinking reaction was allowed to take place for 24 h at 37 °C. After complete crosslinking, the construct was immersed in 50 mM trisodium citrate solution for 24 h to allow alginate dissolution, sonicated and washed with distilled water.

After alginate dissolution, an inlet and outlet needle (21 G) were manually connected to the obtained channel and trisodium citrate solution was flushed into the channel to wash the dissolved alginate. Rhodamine-6G solution (used to dye the solution) was flown inside the channel to check the effective solution flow inside the channel and to investigate the morphology of the obtained hollow channel inside GEL_bulk and GEL_porous scaffolds.

2.5. Gelatin hydrogel scaffolds characterization

Gelatin hydrogels produced with (GEL_porous) and without (GEL_bulk) embedded alginate microbeads were characterized to investigate their suitability as scaffolds for AT engineering.

*Percentage porosity*

The gelatin hydrogels apparent density ρ was calculated as ratio of the weight of anhydrous hydrogels specimens (n = 5) to their volume. The percentage porosity was then calculated according to (2):

$$\text{Porosity } [\%] = \frac{\rho_{GEL\_bulk} - \rho_{GEL\_porous}}{\rho_{GEL\_bulk}} \times 100 \qquad (2)$$

*Morphological characterization*

Scaffolds morphology was evaluated by Scanning Electron Microscopy (SEM) and histological analysis. SEM was performed on GEL_bulk and GEL_porous samples (n = 3, Ø = 6 mm) frozen overnight at -80 °C and lyophilized before observation. Then, the surface and the section of the specimens were observed by SEM (ZEISS Merlin High-resolution SEM) in secondary electron detection mode (1 kV, 100 pA) at 60X magnification. Histological analysis was performed on GEL_bulk and GEL_porous samples embedded in Ultrafreeze® Freeze Gel (Cancer Diagnostic Inc.) and frozen overnight at -80 °C. Then, 6 µm-thick slices were cut by a cryotome, stained by hematoxylin and eosin (H&E) staining to identify the gelatin hydrogel and observed by optical microscope (Nikon Eclipse TE2000, equipped with DS-Fi3 Camera) at 10X magnification.

*Stability and weight variation*

The stability and weight variation of GEL_bulk and GEL_porous samples were evaluated by water uptake tests. Anhydrous specimens (n = 6 per formulation) were weighted ($w_0$), put in 24-multiwell, immersed in 2 mL of $NaN_3$ 0.02% w/v distilled water solution, sealed and stored at 37 °C. At fixed time points (i.e., 30 min, 1, 2, 3, 6 h, 1, 2, 3 days, 1, 2, 3, 4 weeks), specimens were removed from water, gently swabbed and weighted ($w_t$). The average weight variation (ΔW%) was then represented in function of time according to (3):

$$\Delta W\% = \frac{W_t - W_0}{W_0} \times 100 \qquad (3)$$

*Compressive mechanical properties*

The compressive mechanical properties of GEL_bulk and GEL_porous samples (n = 4 per formulation) were tested by Dynamic Mechanical Analyzer (DMA Q800, TA Instruments), equipped with compression clamps.

Tests were conducted at 37 °C with a preload of 0.001 N; a strain-controlled ramp was applied at a 1% $min^{-1}$ rate until 30% strain was reached, then, an unload phase was applied at a 2.5% $min^{-1}$ rate until 1% strain was reached. Native AT samples were obtained from subcutaneous porcine AT and tested on the same day of the animal sacrifice, as comparison. The mechanical parameters calculated from the hysteresis cycle were the elastic modulus (E, measured as the slope in the 1-5% strain range, $R^2 > 0.9$), the maximum stress ($\sigma_{max}$) and the residual deformation ($\varepsilon_{res}$).

*Enzymatic degradation*

The enzymatic degradation of GEL_bulk and GEL_porous was evaluated by *in vitro* tests using collagenase Type I from *Clostridium Histolyticum* (Worthington Biomedical) [43]. Specimens (n = 3 per type per time point, Ø = 6 mm) were disinfected by immersion overnight in 70% v/v solution, allowed to dry and weighted ($w_0$) in sterile condition. Then, samples were placed in sterile Eppendorf tubes, immersed in 500 µL collagenase solution 1 U/mL in PBS [43] or in PBS, as control, and stored in an orbital shaker incubator (37 °C, 100 rpm). At fixed time points (i.e., 1, 2, 3, 4, 6, 24 and 48 h) samples were washed three times with PBS, frozen, lyophilized and weighted ($w_t$). The residual weight (RW%) was calculated as ratio of the weight at the time point *t* to the initial weight, according to formula (1), and represented in time to investigate the gelatin hydrogels degradation.

2.6. *In vitro* channel cell seeding

The possibility of injecting viable cells inside the obtained hollow channel and the capability of viable cells in colonizing the channel following the designed geometry by adhering to its internal walls was preliminary tested by using human mesenchymal stem cells (hMSC). Cells were derived from consentient patients and expanded in culture with Minimum Essential Medium α (MEM α, ThermoFisher Scientific), 10% v/v Fetal Bovine Serum (MSC FBS, ThermoFisher Scientific), 1% v/v Non-Essential Aminoacids (ThermoFisher Scientific) and 1% v/v Antibiotic-Antimycotic (ThermoFisher Scientific); for the *in vitro* tests, cells were used before passage 5. GEL_bulk specimens (2 x 2 $cm^2$) produced with embedded 3D printed alginate (n = 3) were washed in trisodium citrate for 24 h to obtain a hollow channel, disinfected by immersion in 70% v/v ethanol solution overnight and washed with sterile PBS, both by immersion and PBS flush inside the channel. A hMSCs suspension ($5\times10^5$ cells $mL^{-1}$) was loaded in a sterile syringe and manually injected by a sterile 23 G needle in the channel created in the gelatin hydrogels, until completely filled. Specimens were

put in 6-multiwell tissue culture plastics (TCPS) and cultured (37 °C, 5% $CO_2$) for 1 day with 5 mL of culture medium in static conditions. After 1 day, LIVE/DEAD staining was used to qualitatively evaluate the viability of hMSCs seeded inside the channel. First, PBS was gently flushed inside the channel to remove culture medium. Then, a 2 μM Calcein-AM (ThermoFisher Scientific) and 4 μM Ethidium Homodimer-1 (ThermoFisher Scientific) solution was injected inside the channel and specimens were incubated for 40 min. After that, PBS was gently injected inside the channel and specimens were finally observed by fluorescence microscope (Nikon Eclipse TE2000) equipped with Andor Zyla 5.5 Camera (Andor). The percentage of viable cells was calculated as ratio of the number of viable cells to the total number of counted cells according to [44], considering random areas (n = 3) of the samples:

$$\text{Viable cells [\%]} = \frac{N_{\text{green cells}}}{N_{\text{green cells}}+N_{\text{red cells}}} \times 100$$

where $N_{\text{green cells}}$ and $N_{\text{red cells}}$ are the number of counted viable and dead cells, respectively.

### 2.7. *In vitro* human MSCs interaction

GEL_bulk and GEL_porous samples (Ø = 6 mm) were disinfected by immersion overnight in 70% v/v ethanol solution and subsequently washed with sterile PBS to eliminate possible residues of ethanol. Before hMSCs seeding, GEL_bulk and GEL_porous specimens were preconditioned by immersion for 1 h in culture medium (i.e., expansion or adipogenic medium, as subsequently described). hMSCs ($1\times10^5$ cells/sample) were seeded on GEL_bulk, GEL_porous and in 24-multiwell TCPS, as control, and cultured (37 °C, 5% $CO_2$) for 21 days in 2 mL of culture medium; medium was replaced three times per week. For the experiment, cells (i.e., on gelatin scaffolds and TCPS, as control) were kept in culture either in expansion or adipogenic differentiation medium. Expansion medium was composed by Dulbecco's Modified Eagle's Medium (DMEM – low glucose, Sigma Aldrich), 10% v/v FBS, 1% v/v Non-Essential Aminoacids, 1% v/v Antibiotic-Antimycotic; adipogenic medium was composed by DMEM – high glucose, 10% v/v FBS, 1 μm Dexamethasone, 0.01 mg $mL^{-1}$ Insulin, 0.5 mM 3-Isobutyl-1-Methylxanthine (IBMX,) and 100 μg $mL^{-1}$ indomethacin [45].

The metabolic activity of hMSCs cultured on TCPS, GEL_bulk and GEL_porous, either in expansion or adipogenic medium, was checked by Alamar Blue™ assay after 1, 3, 7, 14 and 21 days of culture (n = 4 samples per type, per culture condition) [46]. At each time point, culture medium was replaced with 2 mL of Alamar Blue™ 10% v/v solution either in expansion or adipogenic medium, and cells were incubated (37

°C, 5% $CO_2$) for 4 h; at each time point, Alamar Blue™ solution was also incubated with samples kept in medium in the incubator without cells, as controls. After 4 h, 100 µL were taken from each well (in triplicate), transferred to a 96-multiwell and fluorescence ($\lambda_{excitation}$ = 540 nm, $\lambda_{emission}$ = 595 nm) was read (Tecan, Genius Plus plate reader). The metabolic activity of hMSCs was then represented by the average fluorescence at each time point, subtracting the fluorescence of the respective samples without cells, used as controls. Samples were then washed with PBS and incubated (37 °C, 5% $CO_2$) with 2 mL of fresh culture medium until the subsequent time point. Viable hMSCs cultured on TCPS, GEL_bulk and GEL_porous were qualitatively visualized after 14 days of culture, either in expansion or adipogenic medium, by LIVE/DEAD staining. Samples (n = 3 per type, per culture medium) were washed twice with PBS and incubated with 2 mL of 2 µM Calcein-AM solution and 4 µM Ethidium Homodimer-1 for 40 min. Then, samples were washed with PBS and observed by fluorescence microscope equipped with Andor Zyla 5.5 Camera.

*Adipogenic differentiation*

The adipogenic differentiation of hMSCs was qualitatively checked after 21 days of culture by Oil Red O staining. The Oil Red O stock solution was prepared by dissolving 0.3% w/v Oil Red O powder (Sigma Aldrich) in isopropanol. Samples (n = 3 per type, per culture medium) were washed with PBS, fixed for 30 min in formalin and washed with PBS. The Oil Red O working solution was prepared fresh by mixing 2 parts of stock solution with 3 parts of distilled water, subsequently filtered. Samples were immersed in 2 mL of working solution for 1 h, washed with distilled water and observed by optical microscopy (Nikon Eclipse TE2000) equipped with DS-Fi3 Camera (Nikon) to check hMSCs morphology and the accumulation of red-stained lipid droplets.

### 2.8. *Ex vivo* blood flow

Gelatin hydrogels with a prevascular channel were prepared to test *ex vivo* the diffusion of blood inside the channel, to mimic a possible *in vivo* connection to the human vascular system. To facilitate the scaffold anastomosis procedure, alginate was 3D printed (20 kPa, 21 G, 1 mm $s^{-1}$) so to obtain a channel with saturable dimensions (i.e., Ø > 1 mm). We procured arterial blood vessels from rats discarded as part of other studies (Sprague Dawley rats, ~250 gr., male; Charles River Laboratories, Wilmington, MA). Briefly, 15 – 20 mm long sections of the abdominal aorta of donor rats (Ø = 2 mm) were procured under a surgical microscope. The sections were flushed with sterile saline solution (0.9% NaCl) using a small cannula, and

preserved in the same solution at 4 °C. The sections were then partially inserted in the terminal end of the channel within gelatin scaffold, leaving approximately 5 – 10 mm of the vessel outside the scaffold, in order to act as vascular inlet. The vessel was secured to the gelatin hydrogel using a surgical glue (Vetbond Tissue Adhesive, 3M, Maplewood, MN), without the need for any surgical suture. Then, a cannula was inserted in the vessel sutured to the inlet channel of the vascularizable gelatin scaffold. The cannula was finally connected by a silicon tube to a syringe, filled with pig blood (porcine whole blood Na heparin, Innovative Research™) mounted on a syringe pump and blood was perfused inside the gelatin hollow channel at 70 mL $h^{-1}$.

### 2.9. Statistical analysis

All data are presented as mean ± standard deviation (N ± SD). Data were analyzed by one-way ANOVA tests using GraphPad Prism software; one-way ANOVA on repeated measures was used for the Alamar Blue tests. In the statistical analysis, $p < 0.05$ was considered as statistically different.

## 3. Results

### 3.1. Vascularizable gelatin hydrogels

Micropores in gelatin hydrogels were obtained by embedding alginate microbeads during gelatin hydrogel synthesis (Figure 1A.*i*). The coaxial flow setup (Figure1B.*i*) allowed for a quick and ease production of spherical microbeads (Figure 1B.*ii*) with diameter in 320 – 500 μm range (Figure 1B.*iv*) – with more than 80% of the microbeads possessing a diameter in the 380 – 460 μm range. NaCl 50 mM and trisodium citrate 50 mM were tested as solutions to remove alginate microbeads, using distilled water as control, by measuring weight variation of microbeads in the tested solution (Figure 1B.*iii*). NaCl solution was tested due to its ability to promote exchange of $Na^+$ and $Ca^{2+}$ ions, thus promoting alginate dissolution, and trisodium citrate was tested because of its known $Ca^{2+}$ ions chelator effect. After 20 min of immersion either in water or NaCl 50 mM, the microbeads residual weight was higher than 80%, while after 20 min of immersion in trisodium citrate 50 mM solution, microbeads completely dissolved. These results allowed identifying trisodium citrate 50 mM as optimal solution to promote a quick selective dissolution of the alginate hydrogel microbeads [47].

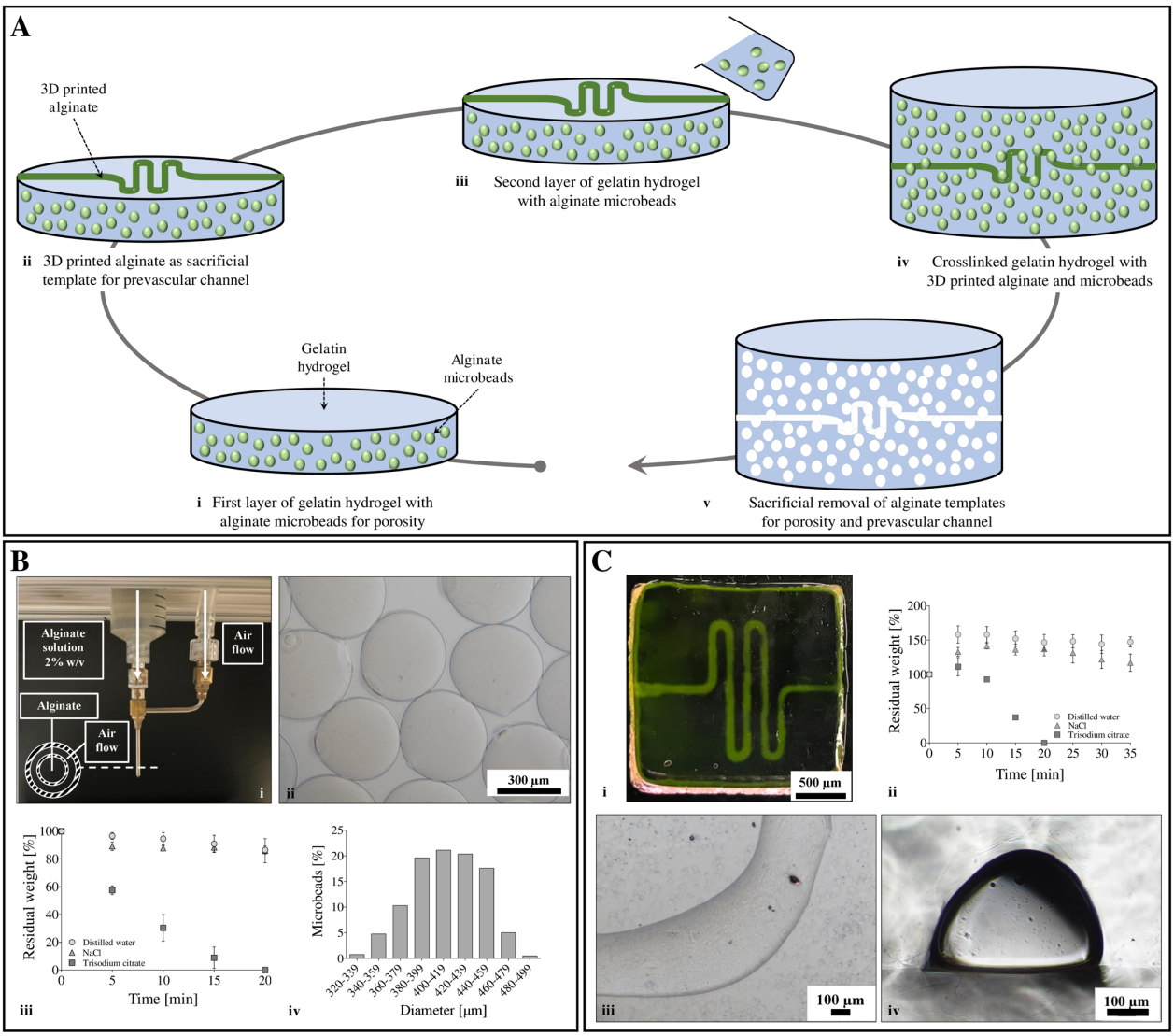


**Figure 1.** **(A)** Fabrication of tissue-mimicking porous gelatin scaffolds with embedded prevascular channel. (*i*) Alginate microbeads (green circles) are embedded in gelatin solution (light blue) during its crosslinking. Then, (*ii*) the gelatin hydrogel is used as substrate for the printing of an alginate filament (green line) that is then ionically crosslinked by $CaCl_2$. (*iii*) A second gelatin solution, loaded with alginate microbeads, is poured on the alginate filament printed on the first layer of gelatin. At the end of this process, (*iv*) a gelatin hydrogel with embedded alginate microbeads and printed filament is obtained. (*v*) The structure is finally immersed in trisodium citrate solution to selectively and simultaneously dissolve alginate microbeads and 3D printed filament to obtain pores (white circles) and a hollow channel (white line) inside the gelatin hydrogel scaffold. **(B)** Alginate microbeads production. (*i*) 2% w/v alginate solution is pumped through a needle by applying an external coaxial air flow to obtain (*ii*) alginate microbeads crosslinked by collection in 100 mM $CaCl_2$ solution. Crosslinked alginate microbeads (*iv*) diameter distribution (n = 400) and (*iii*) dissolution in distilled water, NaCl 50 mM and trisodium citrate 50 mM (n = 3). **(C)** 3D printed sacrificial alginate channel. (*i*) Macroscopic appearance of Rhodamine-G solution flown inside the gelatin channel. (*ii*) Dissolution of 3D printed alginate in distilled water, NaCl 50 mM and trisodium citrate 50 mM (n = 3). Optical microscopy image of (*iii*) top-view and (*iv*) the section of gelatin hydrogel with a hollow channel. Data are expressed as N ± SD.

A prevascular channel was obtained inside the gelatin hydrogels by embedding a sacrificial 3D printed alginate hydrogel snake-like filament (Figure1A.*ii*). The printed filaments dimension ranged between 3 mm and 200 µm, depending on the deposition speed and needle dimension used (Supporting Information, Figure

S1); we observed a decrease in the filaments dimension by increasing the deposition speed (from 1 to 10 mm $s^{-1}$) and reducing the needle dimension (from 20 to 23 G). In the post-printing, we observed an average 20% decrease in filaments dimension, due to alginate crosslinking that caused a shrinking of the printed filament [48]. Representative images of alginate hydrogels 3D printed filaments embedded in gelatin scaffolds are shown in Figure 1C.*iii*. The filaments embedded in gelatin are characterized by a diameter ranging from 300 to 400 μm and accurately reproduce the CAD design used for the 3D printing procedure. Similar to microbeads, the residual weight of 3D printed crosslinked alginate hydrogels during the dissolution tests is shown in Figure 1C.*ii*. Corroborating the results obtained for microbeads, alginate hydrogel filaments completely dissolved after 20 min of exposure to trisodium citrate 50 mM (Figure 1C.*ii*), while alginate hydrogel filaments exposed to NaCl 50 mM and water were characterized by a residual weight higher then 100%, effectively absorbing water. The process of embedding 3D printed alginate hydrogel filament (Figure 1A.*iii*-*iv*), and the subsequent removal of the sacrificial alginate material (Figure 1A.*v*) allowed for the fabrication of a functional channel that supports fluid flow and enabled the fabrication of a prevascular channel. Representative videos of the solution flowing inside the channel obtained in gelatin hydrogels produced with (GEL_porous) and without (GEL_bulk) alginate microbeads are shown in Supporting Information (Video S1 and Video S2). A representative image of gelatin hydrogel with the channel filled with Rhodamine-6G solution is shown in Figure 1C.*i*. The dyed solution fills the channel, accurately following the designed snake-like channel geometry. After the complete filling of the channel, Rhodamine-6G can diffuse inside the gelatin hydrogel, as qualitatively shown in Supporting Information (Figure S2), where images of the same gelatin hydrogel sample at different time points are shown. The diffusion in gelatin hydrogels of Rhodamine-6G – used as model molecule for nutrient diffusion [49] – allowed predicting the inter-channel distance required to guarantee a sufficient exchange of metabolite and catabolites in the engineered tissue. A section of the gelatin hydrogel was cut after alginate dissolution to further investigate the obtained hollow channel. In Figure 1C.*iv*, a hole inside the gelatin section can be observed; this hole represents the hollow channel left after 3D printed alginate dissolution and reproduces the dimension of the alginate printed with the selected parameters. Representative microscopy images of Rhodamine-6G solution inside the channel and of the sections of gelatin hydrogels with and without

embedded microbeads are shown in Supporting Information (Figure S3), proving that prevascular channel can be obtained both in GEL_porous and GEL_bulk hydrogels.

### 3.2. Gelatin hydrogels as scaffolds for adipose tissue engineering

*Percentage porosity*

The calculated porosity for GEL_porous was 93 ± 1%, indicating a clear effect of sacrificial alginate microbeads in the fabrication of highly porous gelatin scaffold, with a pore size, distribution and geometry that mimic the one of physiological AT and may enable an efficient colonization of the scaffold during cell seeding, enhance nutrients transport in the hydrogel and promote newly formed tissue ingrowth.

*Morphological characterization*

The morphology of the gelatin hydrogels is shown in Figure 2.

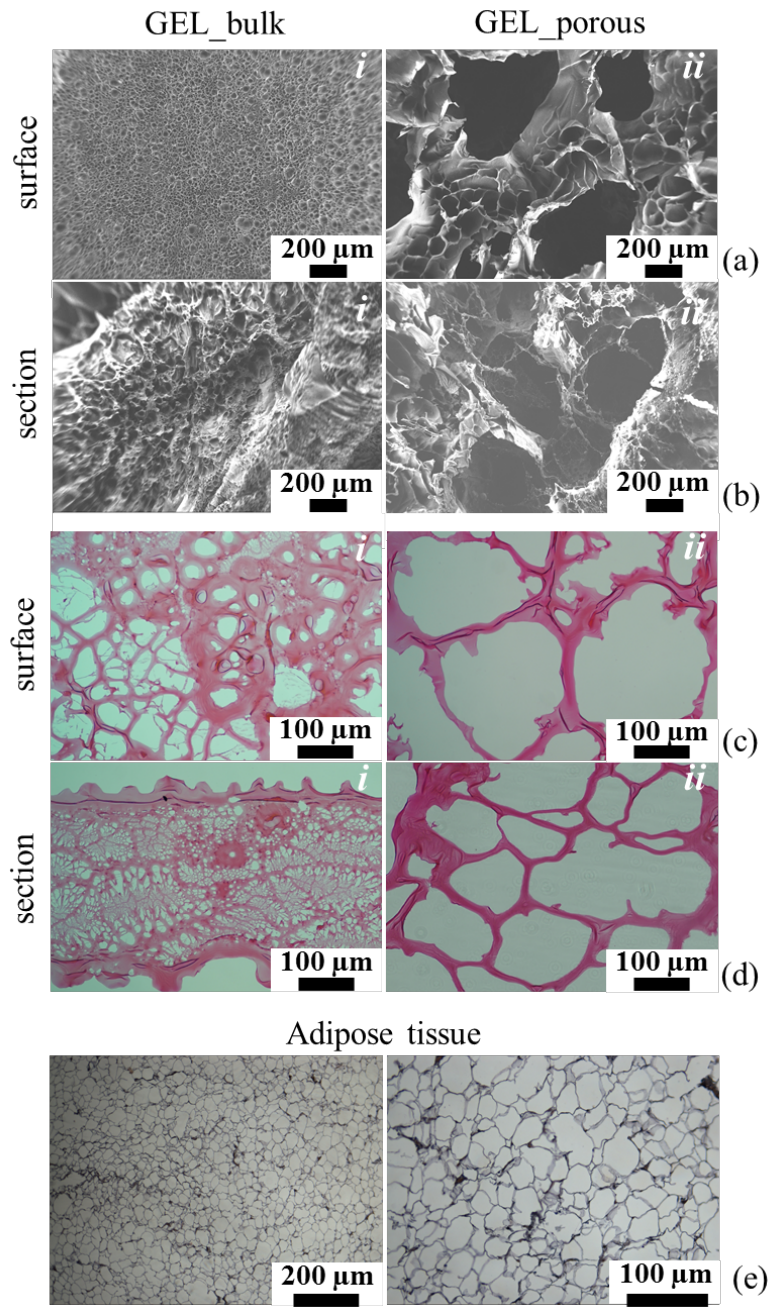


**Figure 2.** Morphological analysis of gelatin hydrogels produced with (GEL_porous) or without (GEL_bulk) embedded alginate microbeads. **(a-b)** SEM micrographs and **(c-d)** H&E histological analysis of (a-c) surface and (b-d) section of (i) GEL_bulk and (ii) GEL_porous. **(e)** Histological sections of decellularized human adipose tissue.

SEM micrographs of the surface and of the section of the gelatin hydrogels are shown in Figure 2a and Figure 2b, respectively. GEL_bulk samples (left column) show a rough and continuous surface, with no evident micropores on the sample surface; similarly, the section of GEL_bulk is characterized by an inhomogeneous morphology of the surface, probably due to the lyophilization procedure used during samples preparation for the SEM analysis, but no evident micropores or pore interconnections can be identified. On the contrary, micrographs of GEL_porous scaffolds depicted the presence of micropores both

at the surface and on the section of the samples, with pores diameters ranging from 200 to 400 μm. These micropores are the voids left from the beads after the removal by immersion in trisodium citrate solution. Similarly, histological sections (Figure 2c and 2d), where the pink areas represent the gelatin hydrogels that absorbed the H&E staining, show a clear difference in the morphology comparing GEL_bulk and GEL_porous. GEL_bulk is characterized by relatively small pores (Ø < 50 μm), which can be given by the freezing procedure used for histological sections preparation. On the contrary, GEL_porous scaffolds show micropores (Ø = 200 – 400 μm), as observed by SEM analysis. Human AT histological sections are shown in Figure 2e, as reference. The morphology of decellularized human AT is comparable to that of GEL_porous samples, whose pores morphology and structure accurately mimic that of human AT; in fact, in AT there are pore walls composed by the AT extracellular matrix that is mimicked, in the proposed scaffold, by the gelatin pore walls obtained in GEL_porous samples after alginate microbeads removal. Despite natural AT is characterized by an average pore size of 50 – 100 μm [50,51], we decided to design our scaffolds with bigger pores dimension (i.e., Ø = 200 – 400 μm), to promote cells infiltration during cells seeding; the pores dimension obtained in GEL_porous is, in fact, optimal for an efficient cells colonization, as demonstrated for other scaffolds proposed in literature [15,22].

Macroscopic images of GEL_bulk and GEL_porous samples after preparation and crosslinking are shown in Figure 3a.*i* and 3a.*ii*; GEL_bulk appears as a transparent gelatin hydrogel, while GEL_porous is characterized by white spots represented by the alginate microbeads, which can be clearly observed by the microscopy image inset, where alginate microbeads appear randomly distributed in the whole gelatin hydrogel.

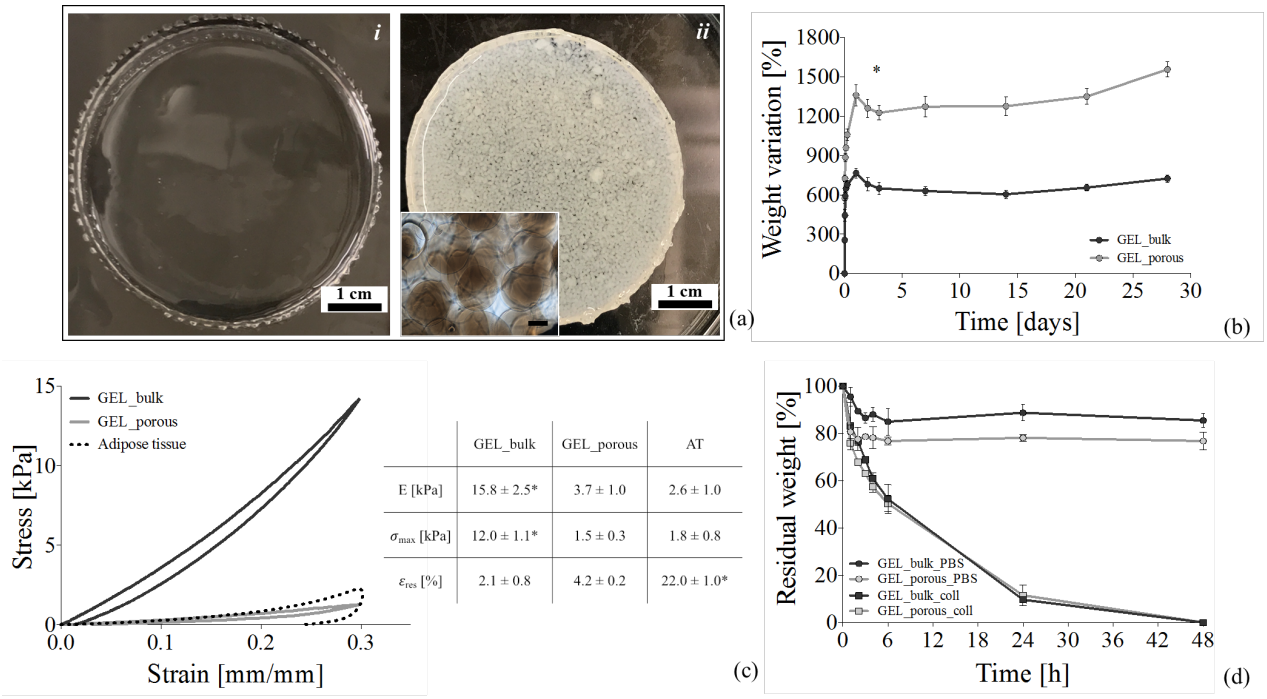


| | GEL_bulk | GEL_porous | AT |
|---|---|---|---|
| E [kPa] | 15.8 ± 2.5* | 3.7 ± 1.0 | 2.6 ± 1.0 |
| $\sigma_{max}$ [kPa] | 12.0 ± 1.1* | 1.5 ± 0.3 | 1.8 ± 0.8 |
| $\varepsilon_{res}$ [%] | 2.1 ± 0.8 | 4.2 ± 0.2 | 22.0 ± 1.0* |

**Figure 3.** Gelatin hydrogels used as scaffolds for adipose tissue engineering. **(a)** Macroscopic images of hydrogels produced (i) without (GEL_bulk) and (ii) with (GEL_porous) embedded alginate microbeads (scale bar: 1 cm; zoomed image scale bar: 100 µm). **(b)** Weight variation in distilled water at 37 °C (n = 6, *p < 0.05 at weight variation plateau) and **(c)** compressive mechanical properties of GEL_bulk, GEL_porous hydrogels and native adipose tissue AT (n = 4; * p < 0.05 comparing one sample to the others). **(d)** *In vitro* enzymatic degradation of GEL_bulk and GEL_porous hydrogels in collagenase type I 1 U/mL in PBS and when compared to pure PBS used as control (n = 3). Data are expressed as N ± SD.

*Stability and weight variation*

Both GEL_bulk and GEL_porous are stable in water at 37 °C, up to 4 weeks (Figure 3b). After 48 h of immersion, both GEL_bulk and GEL_porous reach the swelling plateau phase. After 48 h of immersion (i.e., swelling plateau), GEL_porous shows a weight variation value (ΔW% = 1262 ± 69%) higher ($p < 0.05$) than GEL_bulk (ΔW% = 682 ± 51%), due to the pores obtained after the alginate microbeads sacrificial removal that promote fluids absorption, compared to the more compact hydrogel structure characterizing GEL_bulk.

*Compressive mechanical properties*

A representative curve of the compressive mechanical properties of the hydrogels and the mechanical parameters calculated from stress/strain curves are shown in Figure 3c. Both the hydrogels show a typical viscoelastic response, characterized by a load curve, where the stress increases with increasing applied strain during the compression, and an unload curve, where the stress decreases during the unloading of the sample; the different response during the load and unload phase represent the hysteresis area, index of the energy loss during the mechanical test, which is typical of viscoelastic material and mimics the response of soft human

tissues. The elastic modulus calculated for GEL_ bulk (E = 15.8 ± 2.5 kPa) is statistically different ($p < 0.05$) and higher than the modulus calculated for GEL_porous (E = 3.7 ± 1.0 kPa); similarly, the maximum stress $\sigma_{max}$, representing the stress at the highest compression strain (i.e., 30% compression), was statistically different ($p < 0.05$) and higher for GEL_bulk ($\sigma_{max}$ = 12.0 ± 1.1 kPa) compared to GEL_porous ($\sigma_{max}$ = 1.5 ± 0.3 kPa). The lower mechanical properties identified for GEL_porous are to be attributed to the porous structure and to the higher water content absorbed by GEL_porous during the swelling, compared to GEL_bulk. The mechanical properties obtained for GEL_porous were comparable ($p > 0.05$), in terms of E and $\sigma_{max}$, to those measured for subcutaneous native AT, thus confirming the suitability of GEL_porous in mimicking the mechanical properties of native AT.

*Enzymatic degradation*

The average residual weight of GEL_bulk and GEL_porous samples immersed in 1 U/mL collagenase type I solution in PBS is shown in Figure 3d, using PBS as control. Both GEL_bulk and GEL_porous started losing weight, with comparable trends, after 2 h of exposure to the protease and were characterized by residual weight values lower and statistically different ($p < 0.05$) from the control. After 48 h, samples immersed in PBS show stable residual weight values (i.e., residual weight > 70%), while samples exposed to collagenase type I solution were completely degraded, thus showing a physiological proteolytic degradation for the chemically crosslinked gelatin hydrogels [52].

### 3.3. *In vitro* channel cell seeding

The distribution of viable hMSCs seeded in the channel and stained by LIVE/DEAD after 1 day of culture is representatively shown in Figure 4. Three different areas of the printed design (Figure 4.*i*) are representatively shown. In the images, seeded cells appear spread and uniformly colonized the hollow channel, accurately following the printed design (Figure 4.*ii*). Moreover, viable cells adhered to the inner walls of the obtained hollow channel when considering the cross-section of the seeded channel (Figure 4.*iii*). The calculated percentage cell viability was 92.0 ± 0.7%, with > 90% viable cells detected for all the different considered parts of the channel, confirming that the majority of cells are viable (green cells) and only few dead cells (red cells) are present; the presence of dead cells can be likely referred to the manual procedure used for the seeding that does not allow to control the pressure imposed to the cell suspension and the shear stress acting on the cells.

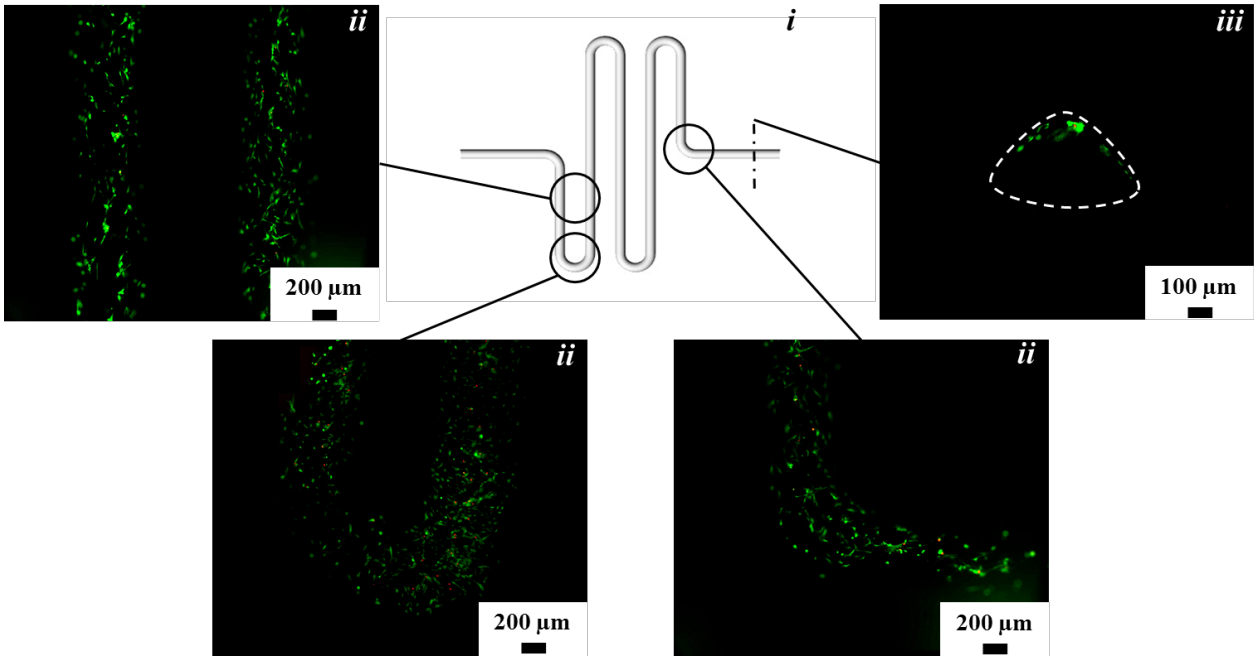


**Figure 4.** *In vitro* cell seeding of the hollow channel obtained in gelatin hydrogels after selective removal of 3D printed alginate. (*i*) Design of the printed structure embedded into gelatin hydrogels and selectively removed and LIVE/DEAD staining of hMSCs seeded inside the channel and cultured for 24 h: (*ii*) top view (scale bar: 200 µm) and (*iii*) section (scale bar: 100 µm).

### 3.4. *In vitro* human mesenchymal stem cell interaction

The metabolic activity (i.e., fluorescence values directly proportional to the metabolic activity of hMSCs) of hMSCs cultured on GEL_bulk, GEL_porous and TCPS (as control), either in expansion and differentiation medium, is shown in Figure 5a.

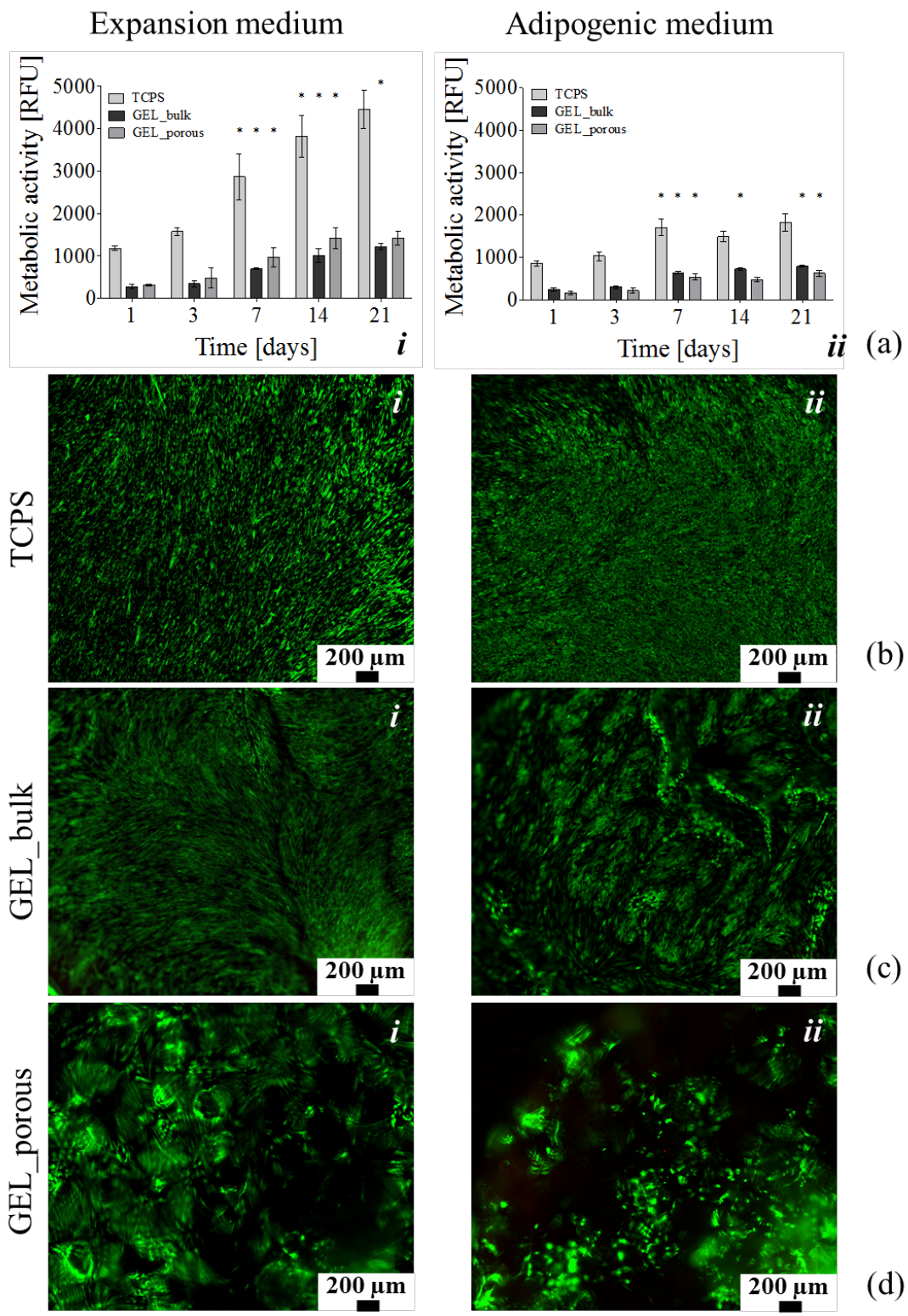


**Figure 5.** *In vitro* cytocompatibility tests with hMSCs seeded on GEL_bulk, GEL_porous and TCPS, as control. **(a)** Metabolic activity measured by Alamar Blue™ of hMSCs cultured in (i) expansion or (ii) adipogenic medium. LIVE/DEAD staining of hMSCs cultured for 14 days in (i) expansion or (ii) adipogenic medium on **(b)** TCPS (as control), **(c)** GEL_bulk and **(d)** GEL_porous (scale bar: 200 µm). (n = 4, *p < 0.05 comparing the same sample at one time point with the previous time point). Data are expressed as N ± SD.

Fluorescence values increased over time for all the tested conditions, evidencing the ability of the gelatin hydrogels in supporting hMSCs proliferation. In particular, hMSCs cultured in expansion medium (Figure 5a.*i*), showed a time-dependent, statistically significant ($p < 0.05$) increase in metabolic activity (i.e., increase of fluorescent signal) on all the substrates investigated. Similar results were obtained for hMSCs cultured in adipogenic medium (Figure 5a.*ii*); for all the considered substrates, a time-dependent, statistically significant ($p < 0.05$) increase in metabolic activity was observed. In general, the absolute fluorescence values were higher when considering hMSCs cultured in expansion medium, compared to cells cultured in adipogenic differentiation medium, as proved by other authors when comparing hMSCs cultured on 2D multiwell plates in expansion vs. adipogenic medium [53]. Although higher absolute fluorescent values were observed for hMSCs cultured on TCPS [54] compared to cells cultured either on GEL_bulk and GEL_porous, the percentage increase of fluorescence obtained comparing 21 days of culture to 1 day of culture, is higher ($p < 0.05$) for the gelatin scaffolds (i.e., 335 ± 29 and 368 ± 46% for GEL_bulk and GEL_porous, respectively) compared to TCPS (i.e., 271 ± 38%). Similarly, when hMSCs are cultured in adipogenic medium, a higher ($p < 0.05$) percentage increase of fluorescence values can be observed after 21 days vs. 1 day comparing GEL_bulk and GEL_porous (162 ± 5 and 196 ± 40%, respectively) to TCPS (111 ± 23%).

The distribution of viable hMSCs was investigated after 14 days of culture by LIVE/DEAD assay (Figure 5b, c and d). Considering all the samples, in both the culture media, the majority of cells (i.e., viable cells > 95%) appeared viable (green cells), with only few red spots (dead cells) visible, confirming the adhesion of viable hMSCs on the gelatin hydrogels during the culture. The cell distribution appears clearly different when comparing GEL_bulk and GEL_porous. hMSCs are spread and randomly distributed on the GEL_bulk samples, as shown in Figure 5c. On the contrary, hMSCs cultured on GEL_porous samples (Figure 5d) appear viable but differently organized, with cells distributed in round circles that represent the pores characterizing the structure of GEL_porous.

*Adipogenic differentiation*

Representative microscopy images of Oil Red O stained cells cultured on (a) TCPS (as control), (b) GEL_bulk (c) and GEL_porous in (*i*) expansion and (*ii*) adipogenic medium are shown in Figure 6.

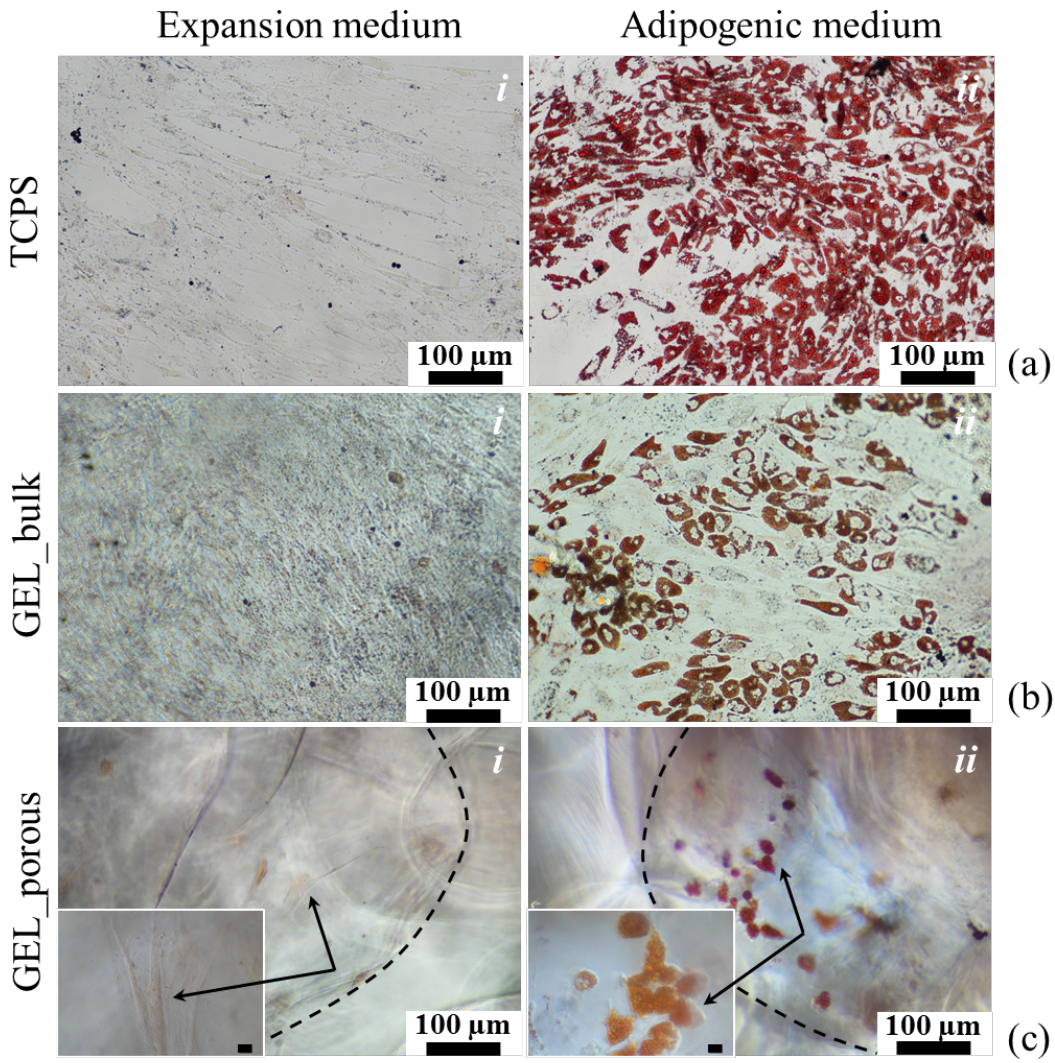


**Figure 6.** *In vitro* cytocompatibility tests with hMSCs seeded on GEL_bulk, GEL_porous and TCPS, as control. Oil Red O staining of hMSCs seeded on **(a)** TCPS (as control), **(b)** GEL_bulk and **(c)** GEL_porous cultured in (i) expansion and (ii) differentiation medium (scale bar: 100 µm; zoomed area scale bar: 10 µm). Arrows indicate cells (elongated cells in Figure 6c.*i* and cells accumulating lipid droplets in Figure 6c.*ii*); dashed lines representatively indicate the edges of pores obtained in GEL_porous samples after alginate microbeads sacrificial removal.

The morphology of cells appeared clearly different comparing the two different culture media used. In both cases, while cells culture on TCPS and GEL_bulk appeared distributed as a cell monolayer, cells cultured on GEL_porous colonized the three-dimensional pores (evidenced by asterisks in Figure 6c) of the porous samples. When cells were cultured in expansion medium (Figure 6.*i*), regardless the culture substrate, cells appeared spread with elongated filopodia (clearly visible in the image inset in Figure 6c.*i*). On the contrary, hMSCs cultured in adipogenic medium possessed a roundish morphology, with dimension in the 30 – 50 µm range; moreover, red-stained lipid droplets accumulated from cells can be clearly observed (evidenced by

dashed lines in Figure 6c). These lipid droplets accumulation is a qualitative and clear sign of differentiation of hMSCs towards the adipogenic phenotype, fundamental requirement for the formation of mature AT.

### 3.5. *Ex vivo* blood flow

E*x vivo* blood flow tests were used to simulate a possible *in vivo* implant of the proposed scaffolds, where the vascularizable gelatin hydrogels would be implanted and connected to the systemic vascular system by anastomosis of the gelatin inlet and outlet channels to the arteriosus and venous system, respectively. Given the difficulties encountered in suturing the vessel to the hydrogel, we decided to test the efficacy of a commercially-available surgical glue (Vetbond Tissue Adhesive, 3M, Maplewood, MN; in patients a similar product is clinically used: Dermabond, Ethicon, Somerville, NJ ) to secure the vessels to the gelatin hydrogel channel without the need for any surgical suture. The use of a surgical glue has the advantage to be less harmful to both the scaffold and the blood vessels, as compared to the use of surgical sutures. In addition, microvascular suturing of small caliber vessels (about 2 – 3 mm in diameter) requires technical expertise and microsurgical equipment that is not always readily available in all clinical settings. Instead, the use of a glue represents a fast, safe, and easy alternative for microvascular anastomosis. In addition, by inserting the vessels within the scaffold (i.e., insertion of ~5 – 10 mm) the possibility of unprecise anastomosis or anastomotic leakages is minimized. Once connected to the cannula and syringe pump, blood could easily flow inside the gelatin scaffold, as shown in the video in Supporting Information (Figure S5, Video S3), completely perfusing the channel obtained inside gelatin hydrogels, thus proving the actual possibility of blood flow inside the channel after scaffolds implantation.

## 4. Discussion

AT defects represent one of the most common consequences of a wide range of medical conditions and trauma, significantly affecting patients' quality of life by impairing their function and/or causing a disfigurement of their body image. Yet, clinically available strategies for AT reconstruction are limited and often characterized by suboptimal effectiveness. In this work, we developed a scaffold with optimal properties to target the regeneration of AT, by coupling a chemically crosslinked gelatin hydrogel, used as scaffolding material, with sacrificial alginate templates, simultaneously in the form of microbeads and 3D printed filaments, to achieve a microporous structure and a prevascular channel by simultaneous removal of

the alginate templates. The integrated approach that we propose to simultaneously obtain porous and vascularizable scaffolds, by using sacrificial structures obtained in different forms (i.e., microbeads and 3D printed filaments) by different fabrication technologies (i.e., microbeads production and 3D printing), is presented here for the first time. The importance of coupling the obtainment of a tissue-mimicking porous structure together with vascularizable channel is generally underestimated, especially when cell-laden hydrogels are used as scaffolding materials. However, tissue-mimicking microporous structures should be obtained when the synthesis process of the scaffold is not compatible with cells embedding, as in the case of this work [55], and could be applied to many other materials. In fact, this procedure could be extended to the production of vascularizable porous scaffolds made of a great variety of synthetic or natural scaffold materials, as long as they are not susceptible to dissolution in trisodium citrate. The fabrication technology we optimized is simple and cost-effective, completely based on the use of natural-derived polymer, and allowed to target the well-established criteria for an optimal AT scaffold production, including adequate physical, biochemical, mechanical and biological properties that would sustain the regeneration of AT while degrading [4], and an effective strategy to promote vascularization [29].

The scaffolding material selected is a crosslinked gelatin hydrogel obtain by *non-zero length* chemical crosslinking, based on a Michael-type reaction between gelatin amino groups and MBA [40]. We selected gelatin, a natural polypeptide derived from partial denaturation of collagen, thanks to its several advantages as scaffolding material, including versatility of fabrication, ease of availability, low price, presence of cell-adhesive motifs (i.e., RGD sequences that promote integrin-mediated interactions), *in vivo* biodegradability and lower immunogenicity and antigenicity compared to collagen [56]. The chemical crosslinking reaction was selected because of its ease and quick procedure (i.e., 24 h required for the gelatin hydrogel production, obtained by simple reagents mixing), production of stable hydrogels in physiological-like condition (i.e., 37 °C, up to 4 weeks), cost-effective overall production, controllable and tunable physico-mechanical properties, previously demonstrated non-cytotoxic effects [41] and potential possible embedding of active biomolecules during the hydrogel preparation [42]. Moreover, the gelatin hydrogel we used was characterized by an oxygen diffusion coefficient of $2.7 \cdot 10^{-5}$ $cm^2$ $s^{-1}$, measured by a procedure describe elsewhere [57], that guarantees a correct oxygen diffusion towards the hydrogel network and a correct oxygen supply to cells adhered to the scaffold, as demonstrated by other authors [58].

A tissue-mimicking microstructure was successfully obtained in the gelatin hydrogel by embedding, at the point of material synthesis, and subsequent sacrificial removal of alginate microbeads, yielding a microporous structure that may promote material transport in the scaffold together with cell colonization and integration with the surrounding tissue, when implanted *in vivo*. This procedure can be easily extended to the production of other scaffolds with differently required pore size by embedding microbeads produced with the desired dimension, by simply changing the parameters used for the microbeads production (i.e., needle size, applied air flow, alginate solution flow rate) [59]. A porosity higher than 90% and pores in the 100 – 400 μm range were obtained in the GEL_porous scaffold, as evidenced both by SEM and histological analysis. The obtained pore size was particularly suitable for the production of scaffolds for AT engineering and similar to that of other scaffolds described for AT engineering, including poly(amidoamine) foams (300 – 500 μm [15]), silk fibroin scaffolds (450 ± 30 μm [20]) and poly (L-glutamic acid) hydrogels (100 – 400 μm [25]). In fact, despite native AT is characterized by smaller pores (Figure 2e), each filled with a single adipocytes, the 100 – 400 μm pore size range is well established as optimal for AT scaffolds production; in fact, previous works demonstrated that this pore size range, compared to smaller pores (i.e., 40 μm) that inhibited cells infiltration and differentiation (i.e., pores too small to promote lipid accumulation) [60], is the optimal to contemporarily promote cells/tissue infiltration and adipogenic differentiation [61].

The obtained scaffold was characterized by mechanical properties (i.e., E = 3 – 4 kPa) suitable for the regeneration of AT (i.e., in particular, subcutaneous AT, E = 2 kPa [27]). In particular, the AT mimicking mechanical properties were achieved by coupling a previously optimized gelatin hydrogel formulation (i.e., gelatin hydrogel concentration and reaction stoichiometry) [41] and the voids left after alginate microbeads sacrificial removal. Mimicking the structural-mechanical properties of AT is of fundamental importance for both stiffness-guided cells-biomaterials interactions and for the replication of a natural feel at touch of the implanted AT scaffolds, as demonstrated by other authors that achieved mechanical properties similar to the here proposed scaffolds either by using decellularized AT (E = 2 – 4 kPa [62]), poly(amidoamine) foams (E = 3 – 4 kPa [15]), hyaluronic acid hydrogels (E = 10 – 20 kPa [16]) or collagen/hyaluronic acid scaffolds (E = 4 – 7 kPa [18]).

The proposed gelatin scaffolds were also demonstrated to be optimal substrates for the proliferation (shown by Alamar Blue assay) and differentiation of hMSCs towards adipocytes (qualitatively shown by Oil Red O

staining), key aspect for the regeneration of fully functional mature AT. The selected cell source (i.e., bone marrow mesenchymal stem cells) were shown in different contexts to be suitable for AT engineering purposes, although different human stem cell populations can be used as sources for the *in vitro* culture and differentiation towards adipogenic phenotype on scaffolds (e.g., stem cells derived from umbilical cord, adipose tissue or bone marrow) [23,63], thus proving the possibility of isolation of hMSCs from patients' bone marrow and culture and adipogenic differentiation on the here proposed scaffold to obtain a viable construct. Moreover, a clear difference in cells distribution was observed by comparing GEL_bulk and GEL_porous samples. In fact, cells appear distributed on the surface of GEL_bulk samples, thus proving the absence of cells colonization within the scaffold, while cells are shown to colonize the pores obtained in GEL_porous scaffolds (Figure 6c); despite cells were shown to colonize the pores of GEL_porous structure, the static cell seeding method used for the *in vitro* tests might limit the infiltration of cells in the porous structure and alternative seeding methods (e.g., dynamic seeding) should be considered to improve the colonization of the scaffold [64]. Moreover, considering the *in vitro* tests, the produced scaffolds were shown to be particularly suitable for long-term *in vitro* cultures (i.e., 21 days), maintaining their dimension and shape as shown in Supporting Information (Figure S4), a key feature when aiming at the regeneration of AT tissue, both from a functional and aesthetic point of view. This result, together with collagenase type I degradation demonstrated by *in vitro* tests, suggests the overall structural stability of the scaffold while allowing for its remodeling. Specifically, we used collagenase type I as *in vitro* protease model. Collagenase type I contains the activity of several proteases, including collagenase, caseinase, clostripain, and trypsin and it is widely used in literature to test collagen or gelatin scaffold enzymatic degradability [43]. Similar enzymatic degradation profiles were detected for gelatin methacryloyl hydrogels [65] and gelatin hydrogels crosslinked by other mechanisms (e.g., glutaraldehyde) [66] that were also shown to sustain long-term *in vivo* implants (i.e., one month), thus proving the possibility of enzymatic degradation for the gelatin hydrogel scaffold here proposed and, possibly, an *in vivo* stability that would allow for AT regeneration while the scaffold is degrading. Degradation of the studied gelatin-based material with collagenase type I suggests that adipocytes, especially during differentiation and proliferation, can remodel the tissue/scaffold by secretion of metalloproteinase (MMP-2 and MMP-9), enzymes with known collagenase and gelatinase activity [67].

Finally, the strategy we adopted to promote the vascularization of the produced gelatin scaffolds is based on an indirect 3D printing approach. This strategy enables the control over the vascular channels spatial distribution and dimension, feature that is hardly achievable when using other vascularization strategies described for AT engineering, including the use of growth factors or cell-based approaches [68,69]. For instance, vascular endothelial growth factors (VEGF) showed to enhance neovascularization of collagen-chitosan scaffolds *in vivo* [70]; similarly, the use of alginate microbeads to control the release of fibroblast growth factor (FGF-1) [71] in collagen gels improved neovascularization in *in vitro* and *in vivo* [72]. In cell-based techniques, enhanced vascularization was observed *in vitro* by co-culture of adipose stromal cells and endothelial cells [73] and of human adipose derived stem cells with human umbilical vein endothelial cells [74]. Enhanced vascularization was also promoted *in vivo* by using human endothelial cells seeded on 3D printed poly(D,L)-lactide polymer [75] and human adipose derived stem cells spheroids [25]. However, in the considered strategies, a randomly distributed vascular network is obtained, while the indirect 3D printing strategy we adopted here allowed for a fine control over the geometrical distribution of the vascular channel to be formed (i.e., snake-like channel obtained in the gelatin hydrogel), thus allowing for a fine design and engineering of the vascular structure to be embedded in the hydrogel. Moreover, our strategy allows for a design that eases the access for surgeons to anastomosis sites for the connection of the scaffold to the vascular system of the patient after *in vivo* implantation [76], as demonstrated by the on bench test we performed by anastomosis to a rat's vessel. The anastomosis to the patient's own vascular system at the time of the implant allows for immediate nutrients support to the cells populating the scaffold, as demonstrated for decellularized scaffolds implanted *in vivo* in rats by side-to-end anastomosis to the aorta abdominalis and to the vena cava [77], thus avoiding the time required for the formation of the vascular system affecting the previously cited methods (i.e., 6-8 weeks [70,72]), which may lead to cell suffering, death and necrotic core formation.

When using indirect 3D printing, the formation of an open vascular lumen is a stringent requirement. In this work, we demonstrated that, by sacrificial removal of the 3D printed snake-like alginate filament, we were able to obtain a hollow vascular channel that allowed for the flow of both water (Rhodamine-6G dyed solution) – used to have an ease and clear detection of the obtained channel shape – and porcine blood – used to test the flow of a liquid with properties similar to human blood. Moreover, despite long-term tests would

be required to investigate the stability of the obtained channel, the stable weight and dimension of the gelatin hydrogel observed during the *in vitro* culture would also promote the stability of the obtained lumen inside the hydrogel. Additionally, *in vitro* tests showed that hMSCs can adhere to the channel walls and colonize them. The 3D printing strategy we adopted allows for the control of the dimension of the channels, useful when aiming at obtaining vascular networks suitable for different body sites. The smallest channels we were able to obtain and handle (i.e., easy connection by needles to flow a solution inside the channels) were of 300 – 400 μm, obtained in the GEL_bulk samples; however, for GEL_porous samples and gelatin scaffolds used for *ex vivo* blood flow tests, we decided to change the printing parameters to obtain larger channels (i.e., Ø > 1 mm) because of the difficulties encountered in connecting the channel of GEL_porous samples to the syringe pump and to give surgeons accessible and suturable sites for anastomosis. The dimension of the channel we obtained was comparable to that obtained by some other authors that used sacrificial networks by 3D printing technology, including sacrificial carbohydrate glass (i.e., 150 – 750 μm [34]) or Pluronic F127 (i.e., 150 – 650 μm [37]), and smaller compared to other used sacrificial materials, including gelatin (i.e., 0.7 – 1.5 mm [33]), polyisocyanide (i.e., > 2 mm [78]) or PVA (i.e., > 2 mm [38]). For even smaller vessels, however, other fabrication technologies, including micromolding and electrospinning, have to be used [79–81]. The choice of alginate as sacrificial material is optimal, thanks to the known biocompatible and bioinert properties; moreover, alginate could be used as delivery system of growth factors to further increase the vascularization of the scaffolds [72]. The dissolution of alginate by using trisodium citrate is also a safety procedure; in fact, despite the samples are washed with water after alginate dissolution, the presence of residual trisodium citrate has to be considered safe, since this salt is routinely used in clinics (e.g., blood transfusion) and it is physiologically quickly metabolized by mammalian cells in the Kreb's cycle (e.g., 3 g of trisodium citrated metabolized by human liver in 5 min) [82]; thus, for a total breast implant, the quantity of trisodium citrate used for the production of our scaffolds would be potentially metabolized by a healthy patient in roughly 1 h, thus allowing the successful integration of the scaffold to the patient's vascular system. Moreover, thanks to the possibility of controlling the printed alginate filaments dimension by varying the printing parameters (Figure S1), hierarchical channels characterized by different dimensions, more representative of the *in vivo* vascular network, might be obtained [83,84]. Additionally, the prevascular network may not only allow for an enhanced transport of metabolites and catabolites throughout the whole

scaffolds, but also as a support, during mature tissue growth and scaffolds remodeling, for the formation of angiogenic sprouts [33]. When considering the section of the samples, we identified completely open lumens. However, the obtained lumen geometry was not circular but more elliptical, probably due to the printing of alginate filaments on an already crosslinked gelatin layer; in fact, printed alginate filaments spread on the printing substrate and are subsequently characterized by an elliptical shape once printed, as already reported and discussed from other authors that adopted similar vascularization strategies [33].

## 5. Conclusions

Vascularizable crosslinked gelatin porous scaffolds were obtained by means of simultaneous sacrificial removal of alginate microbeads, used to obtain randomly distributed porosity, and 3D printed alginate hydrogels, used to obtain a vascular channel with controlled geometrical distribution. The tissue-mimicking microporous gelatin hydrogels were suitable as scaffolds for AT engineering in terms of porosity, mechanical properties, enzymatic degradability and ability to support hMSCs proliferation and differentiation towards an adipogenic phenotype. At the same time, a perfusable hollow vascular channel was obtained in the gelatin scaffolds and were successfully connected *ex vivo* to blood vessels to form a successfully perfused system, useful to subsequently promote scaffold vascularization and possible successful *in vivo* clinical application of the scaffold.

**Acknowledgement**

BM acknowledges a Paul M. Cook Career Development Professorship and a REED Award for the partial support of the study. NCN was financially supported by a Progetto Roberta Rocca (Doctoral at MIT) Fellowship. MB was partially supported by a MIT-France Program.

**References**


[1] T. Ronti, G. Lupattelli, E. Mannarino, The endocrine function of adipose tissue: An update, Clin. Endocrinol. (Oxf). 64 (2006) 355–365. doi:10.1111/j.1365-2265.2006.02474.x.

[2] P. Gómez-Campelo, C. Bragado-Álvarez, M.J. Hernández-Lloreda, Psychological distress in women with breast and gynecological cancer treated with radical surgery, Psychooncology. 466 (2014) 459–466. doi:10.1002/pon.3439.

[3] C.T. Gomillion, K.J.L. Burg, Stem cells and adipose tissue engineering, Biomaterials. 27 (2006) 6052–6063. doi:10.1016/j.biomaterials.2006.07.033.

[4] I. Van Nieuwenhove, L. Tytgat, M. Ryx, P. Blondeel, F. Stillaert, H. Thienpont, H. Ottevaere, P. Dubruel, S. Van Vlierberghe, Soft tissue fillers for adipose tissue regeneration: From hydrogel development toward clinical applications, Acta Biomater. 63 (2017) 37–49. doi:10.1016/j.actbio.2017.09.026.

[5] A. Casadei, R. Epis, L. Ferroni, I. Tocco, C. Gardin, E. Bressan, S. Sivolella, V. Vindigni, P. Pinton, G. Mucci, B. Zavan, Adipose tissue regeneration: A state of the art, J. Biomed. Biotechnol. (2012) 1–12. doi:10.1155/2012/462543.

[6] F. Lu, J. Li, J. Gao, R. Ogawa, C. Ou, B. Yang, B. Fu, Improvement of the Survival of Human Autologous Fat Transplantation by Using VEGF-Transfected Adipose-Derived Stem Cells, Plast. Reconstr. Surg. 124 (2009) 1437–1446. doi:10.1097/PRS.0b013e3181babbb6.

[7] C. Hillard, J.D. Fowler, R. Barta, B. Cunningham, Silicone breast implant rupture: a review, Gland Surg. 6 (2017) 163–168. doi:10.21037/gs.2016.09.12.

[8] M.Y. Nahabedian, K. Patel, Autologous flap breast reconstruction: Surgical algorithm and patient selection, J. Surg. Oncol. 113 (2016) 865–874. doi:10.1002/jso.24208.

[9] R.K. Khouri, R.-E.R. Khouri, J.R. Lujan-Hernandez, K.R. Khouri, L. Lancerotto, D.P. Orgill, Diffusion and Perfusion: The Keys to Fat Grafting, Plast. Reconstr. Surg. Glob. Open. 2 (2014) e220. doi:10.1097/GOX.0000000000000183.

[10] S.W. Cho, S.S. Kim, J. Won Rhie, H. Mi Cho, C. Yong Choi, B.S. Kim, Engineering of volume-stable adipose tissues, Biomaterials. 26 (2005) 3577–3585. doi:10.1016/j.biomaterials.2004.09.013.

[11] R.M. Shanti, S. Janjanin, W.-J. Li, L.J. Nesti, M.B. Mueller, M.B. Tzeng, R.S. Tuan, In vitro adipose

tissue engineering using an electrospun nanofibrous scaffold., Ann. Plast. Surg. 61 (2008) 566–571. doi:10.1097/SAP.0b013e31816d9579.

[12] M. Neubauer, M. Hacker, P. Bauer-Kreisel, B. Weiser, C. Fischbach, M.B. Schulz, A. Goepferich, T. Blunk, Adipose tissue engineering based on mesenchymal stem cells and basic fibroblast growth factor in vitro., Tissue Eng. 11 (2006) 1840–51. doi:10.1089/ten.2005.11.1840.

[13] P.N. Patel, C.K. Smith, C.W. Patrick, Rheological and recovery properties of poly(ethylene glycol) diacrylate hydrogels and human adipose tissue, J. Biomed. Mater. Res. - Part A. 73 (2005) 313–319. doi:10.1002/jbm.a.30291.

[14] F.P. Brandl, A.K. Seitz, J.K.V. V Teßmar, T. Blunk, A.M. Göpferich, Enzymatically degradable poly(ethylene glycol) based hydrogels for adipose tissue engineering, Biomaterials. 31 (2010) 3957–3966. doi:10.1016/j.biomaterials.2010.01.128.

[15] E. Rossi, I. Gerges, A. Tocchio, M. Tamplenizza, P. Aprile, C. Recordati, F. Martello, I. Martin, P. Milani, C. Lenardi, Biologically and mechanically driven design of an RGD-mimetic macroporous foam for adipose tissue engineering applications, Biomaterials. 104 (2016) 65–77. doi:10.1016/j.biomaterials.2016.07.004.

[16] M. Fan, Y. Ma, Z. Zhang, J. Mao, H. Tan, X. Hu, Biodegradable hyaluronic acid hydrogels to control release of dexamethasone through aqueous Diels-Alder chemistry for adipose tissue engineering, Mater. Sci. Eng. C. 56 (2015) 311–317. doi:10.1016/j.msec.2015.04.004.

[17] A. Borzacchiello, L. Mayol, P.A. Ramires, A. Pastorello, C. Di Bartolo, L. Ambrosio, E. Milella, Structural and rheological characterization of hyaluronic acid-based scaffolds for adipose tissue engineering, Biomaterials. 28 (2007) 4399–4408. doi:10.1016/j.biomaterials.2007.06.007.

[18] N. Davidenko, J.J. Campbell, E.S. Thian, C.J. Watson, R.E. Cameron, Collagen-hyaluronic acid scaffolds for adipose tissue engineering, Acta Biomater. 6 (2010) 3957–3968. doi:10.1016/j.actbio.2010.05.005.

[19] S.P. Hoo, Q.L. Loh, Z. Yue, J. Fu, T.T.Y. Tan, C. Choong, P.P.Y. Chan, Preparation of a soft and interconnected macroporous hydroxypropyl cellulose methacrylate scaffold for adipose tissue engineering, J. Mater. Chem. B. 1 (2013) 3107. doi:10.1039/c3tb00446e.

[20] J.R. Mauney, T. Nguyen, K. Gillen, C. Kirker-Head, J.M. Gimble, D.L. Kaplan, Engineering adipose-

like tissue in vitro and in vivo utilizing human bone marrow and adipose-derived mesenchymal stem cells with silk fibroin 3D scaffolds, Biomaterials. 28 (2007) 5280–5290. doi:10.1016/j.biomaterials.2007.08.017.

[21] B. Huber, K. Borchers, G.E.M.E. Tovar, P.J. Kluger, Methacrylated gelatin and mature adipocytes are promising components for adipose tissue engineering., J. Biomater. Appl. 30 (2016) 699–710. doi:10.1177/0885328215587450.

[22] K.H. Chang, H.T. Liao, J.P. Chen, Preparation and characterization of gelatin/hyaluronic acid cryogels for adipose tissue engineering: In vitro and in vivo studies, Acta Biomater. 9 (2013) 9012–9026. doi:10.1016/j.actbio.2013.06.046.

[23] L. Liu, H. Liu, M. Chen, S. Ren, P. Cheng, H. Zhang, MiR-301b~miR-130b-PPARγ axis underlies the adipogenic capacity of mesenchymal stem cells with different tissue origins, Sci. Rep. 7 (2017) 1–8. doi:10.1038/s41598-017-01294-2.

[24] J.H. Choi, J.M. Gimble, K. Lee, K.G. Marra, J.P. Rubin, J.J. Yoo, G. Vunjak-Novakovic, D.L. Kaplan, Adipose Tissue Engineering for Soft Tissue Regeneration, Tissue Eng. Part B Rev. 16 (2010) 413–426. doi:10.1089/ten.teb.2009.0544.

[25] K. Zhang, L. Song, J. Wang, S. Yan, G. Li, L. Cui, J. Yin, Strategy for constructing vascularized adipose units in poly(L-glutamic acid) hydrogel porous scaffold through inducing in-situ formation of ASCs spheroids, Acta Biomater. 51 (2017) 246–257. doi:10.1016/j.actbio.2017.01.043.

[26] L. Hong, I. Peptan, P. Clark, J.J. Mao, Ex vivo adipose tissue engineering by human marrow stromal cell seeded gelatin sponge, Ann. Biomed. Eng. 33 (2005) 511–517. doi:10.1007/s10439-005-2510-7.

[27] N. Alkhouli, J. Mansfield, E. Green, J. Bell, B. Knight, N. Liversedge, J.C. Tham, R. Welbourn, A.C. Shore, K. Kos, C.P. Winlove, The mechanical properties of human adipose tissues and their relationships to the structure and composition of the extracellular matrix., Am. J. Physiol. Endocrinol. Metab. 305 (2013) E1427-35. doi:10.1152/ajpendo.00111.2013.

[28] B. Vailhé, D. Vittet, J.J. Feige, In vitro models of vasculogenesis and angiogenesis, Lab. Investig. 81 (2001) 439–452. doi:10.1038/labinvest.3780252.

[29] E.C. Novosel, C. Kleinhans, P.J. Kluger, Vascularization is the key challenge in tissue engineering, Adv. Drug Deliv. Rev. 63 (2011) 300–311. doi:10.1016/j.addr.2011.03.004.

[30] T. Takei, S. Sakai, T. Ono, H. Ijima, K. Kawakami, Fabrication of Endothelialized Tube in Collagen Gel as Starting Point for Self-Developing Capillary-Like Network to Construct Three-Dimensional Organs In Vitro, Biotechnol. Bioeng. 95 (2006) 1–7. doi:10.1002/bit.

[31] G. Voros, E. Maquoi, D. Demeulemeester, N. Clerx, D. Collen, H.R. Lijnen, Modulation of angiogenesis during adipose tissue development in murine models of obesity, Endocrinology. 146 (2005) 4545–4554. doi:10.1210/en.2005-0532.

[32] V.K. Lee, A.M. Lanzi, H. Ngo, S.S. Yoo, P.A. Vincent, G. Dai, Generation of multi-scale vascular network system within 3D hydrogel using 3D bio-printing technology, Cell. Mol. Bioeng. 7 (2014) 460–472. doi:10.1007/s12195-014-0340-0.

[33] V.K. Lee, D.Y. Kim, H. Ngo, Y. Lee, L. Seo, S.-S.S. Yoo, P.A. Vincent, G. Dai, Creating perfused functional vascular channels using 3D bio-printing technology, Biomaterials. 35 (2014) 8092–8102. doi:10.1016/j.biomaterials.2014.05.083.

[34] J.S. Miller, K.R. Stevens, M.T. Yang, B.M. Baker, D.-H.T. Nguyen, D.M. Cohen, E. Toro, A.A. Chen, P.A. Galie, X. Yu, R. Chaturvedi, S.N. Bhatia, C.S. Chen, Rapid casting of patterned vascular networks for perfusable engineered three-dimensional tissues, Nat. Mater. 11 (2012) 768–774. doi:10.1038/nmat3357.

[35] L.E. Bertassoni, M. Cecconi, V. Manoharan, M. Nikkhah, J. Hjortnaes, A.L. Cristino, G. Barabaschi, D. Demarchi, M.R. Dokmeci, Y. Yang, A. Khademhosseini, Hydrogel bioprinted microchannel networks for vascularization of tissue engineering constructs, Lab Chip. 14 (2014) 2202–2211. doi:10.1039/C4LC00030G.

[36] I. Ortega, L. Dew, A.G. Kelly, C.K. Chong, S. MacNeil, F. Claeyssens, Fabrication of biodegradable synthetic perfusable vascular networks via a combination of electrospinning and robocasting, Biomater. Sci. 3 (2015) 592–596. doi:10.1039/C4BM00418C.

[37] D.B. Kolesky, R.L. Truby, A.S. Gladman, T.A. Busbee, K.A. Homan, J.A. Lewis, 3D bioprinting of vascularized, heterogeneous cell-laden tissue constructs, Adv. Mater. 26 (2014) 3124–3130. doi:10.1002/adma.201305506.

[38] S. Li, Y.Y. Liu, L.J. Liu, Q.X. Hu, A Versatile Method for Fabricating Tissue Engineering Scaffolds with a Three-Dimensional Channel for Prevasculature Networks, ACS Appl. Mater. Interfaces. 8

(2016) 25096–25103. doi:10.1021/acsami.6b07725.

[39] J.B. Lee, X. Wang, S. Faley, B. Baer, D.A. Balikov, H.J. Sung, L.M. Bellan, Development of 3D Microvascular Networks Within Gelatin Hydrogels Using Thermoresponsive Sacrificial Microfibers, Adv. Healthc. Mater. 5 (2016) 781–785. doi:10.1002/adhm.201500792.

[40] M.C. Tanzi, S. Farè, I. Gerges, Crosslinked Gelatin Hydrogels, WO2012164032 A1, 2014.

[41] N. Contessi Negrini, P. Tarsini, M.C. Tanzi, S. Farè, Chemically Crosslinked Gelatin Hydrogels as Scaffolding Materials for Adipose Tissue Engineering, J. Appl. Polym. Sci. (2018). doi:10.1002/app.47104.

[42] L. Gritsch, F.L. Motta, N. Contessi Negrini, L.H. Yahia, S. Farè, Crosslinked gelatin hydrogels as carriers for controlled heparin release, Mater. Lett. 228 (2018) 375–378. doi:10.1016/j.matlet.2018.06.047.

[43] B. Marelli, D. Le Nihouannen, S.A. Hacking, S. Tran, J. Li, M. Murshed, C.J. Doillon, C.E. Ghezzi, Y.L. Zhang, S.N. Nazhat, J.E. Barralet, Newly identified interfibrillar collagen crosslinking suppresses cell proliferation and remodelling, Biomaterials. 54 (2015) 126–135. doi:10.1016/j.biomaterials.2015.03.018.

[44] N. Contessi Negrini, L. Bonetti, L. Contili, S. Farè, 3D printing of methylcellulose-based hydrogels, Bioprinting. 10 (2018) 1–10. doi:10.1016/j.bprint.2018.e00024.

[45] M.A. Scott, V.T. Nguyen, B. Levi, A.W. James, Current Methods of Adipogenic Differentiation of Mesenchymal Stem Cells, Stem Cells Dev. 20 (2011) 1793–1804. doi:10.1089/scd.2011.0040.

[46] V. Angeloni, N. Contessi, C. De Marco, S. Bertoldi, M. Cristina, M. Grazia, S. Farè, Polyurethane foam scaffold as in vitro model for breast cancer bone metastasis, Acta Biomater. 63 (2017) 306–316. doi:10.1016/J.ACTBIO.2017.09.017.

[47] Z. Wu, X. Su, Y. Xu, B. Kong, W. Sun, S. Mi, Bioprinting three-dimensional cell-laden tissue constructs with controllable degradation, Sci. Rep. 6 (2016) 1–10. doi:10.1038/srep24474.

[48] S.L. Huang, Y.S. Lin, The Size Stability of Alginate Beads by Different Ionic Crosslinkers, Adv. Mater. Sci. Eng. 2017 (2017). doi:10.1155/2017/9304592.

[49] S.P. Zustiak, H. Boukari, J.B. Leach, Solute diffusion and interactions in cross-linked poly(ethylene glycol) hydrogels studied by Fluorescence Correlation Spectroscopy, 6 (2010) 247–253.

doi:10.1039/C0SM00111B.

[50] K. Comley, N.A. Fleck, A micromechanical model for the Young's modulus of adipose tissue, Int. J. Solids Struct. 47 (2010) 2982–2990. doi:10.1016/j.ijsolstr.2010.07.001.

[51] A. Sbarbati, D. Accorsi, D. Benati, L. Marchetti, G. Orsini, G. Rigotti, P. Panettiere, Subcutaneous adipose tissue classification, Eur. J. Histochem. 54 (2010) 48. doi:10.4081/ejh.2010.e48.

[52] X. Zhao, Q. Lang, L. Yildirimer, Z.Y. Lin, W. Cui, N. Annabi, K.W. Ng, M.R. Dokmeci, A.M. Ghaemmaghami, A. Khademhosseini, Photocrosslinkable Gelatin Hydrogel for Epidermal Tissue Engineering, Adv. Healthc. Mater. 5 (2016) 108–118. doi:10.1002/adhm.201500005.

[53] I. Sekiya, B.L. Larson, J.T. Vuoristo, J.-G. Cui, D.J. Prockop, Adipogenic Differentiation of Human Adult Stem Cells From Bone Marrow Stroma (MSCs), J. Bone Miner. Res. 19 (2003) 256–264. doi:10.1359/JBMR.0301220.

[54] E. Sayin, R.H. Rashid, J.C. Rodríguez-Cabello, A. Elsheikh, E.T. Baran, V. Hasirci, Human adipose derived stem cells are superior to human osteoblasts (HOB) in bone tissue engineering on a collagen-fibroin-ELR blend, Bioact. Mater. 2 (2017) 71–81. doi:10.1016/j.bioactmat.2017.04.001.

[55] A. Tocchio, M. Tamplenizza, F. Martello, I. Gerges, E. Rossi, S. Argentiere, S. Rodighiero, W. Zhao, P. Milani, C. Lenardi, Versatile fabrication of vascularizable scaffolds for large tissue engineering in bioreactor, Biomaterials. 45 (2015) 124–131. doi:10.1016/j.biomaterials.2014.12.031.

[56] S. Gorgieva, V. Kokol, Collagen- vs. Gelatine-Based Biomaterials and Their Biocompatibility: Review and Perspectives, in: Biomater. Appl. Nanomedicine, 2011: pp. 17–52. doi:10.5772/711.

[57] B. Marelli, M.A. Brenckle, D.L. Kaplan, F.G. Omenetto, Silk Fibroin as Edible Coating for Perishable Food Preservation, Sci. Rep. 6 (2016) 1–11. doi:10.1038/srep25263.

[58] J.E. Valentin, D.O. Freytes, J.M. Grasman, C. Pesyna, J. Freund, T.W. Gilbert, S.F. Badylak, Oxygen diffusivity of biologic and synthetic scaffold materials for tissue engineering, J. Biomed. Mater. Res. - Part A. 91 (2009) 1010–1017. doi:10.1002/jbm.a.32328.

[59] L. Draghi, D. Brunelli, S. Farè, M.C. Tanzi, Programmed cell delivery from biodegradable microcapsules for tissue repair, J. Biomater. Sci. Polym. Ed. 26 (2015) 1002–1012. doi:10.1080/09205063.2015.1070706.

[60] D. Von Heimburg, S. Zachariah, H. Kühling, I. Heschel, H. Schoof, B. Hafemann, N. Pallua, Human

preadipocytes seeded on freeze-dried collagen scaffolds investigated in vitro and in vivo, Biomaterials. 22 (2001) 429–438. doi:10.1016/S0142-9612(00)00186-1.

[61] K. Hemmrich, D. Von Heimburg, R. Rendchen, C. Di Bartolo, E. Milella, N. Pallua, Implantation of preadipocyte-loaded hyaluronic acid-based scaffolds into nude mice to evaluate potential for soft tissue engineering, Biomaterials. 26 (2005) 7025–7037. doi:10.1016/j.biomaterials.2005.04.065.

[62] C. Yu, J. Bianco, C. Brown, L. Fuetterer, J.F. Watkins, A. Samani, L.E. Flynn, Porous decellularized adipose tissue foams for soft tissue regeneration, Biomaterials. 34 (2013) 3290–3302. doi:10.1016/j.biomaterials.2013.01.056.

[63] S. Danti, M. D'Acunto, L. Trombi, S. Berrettini, A. Pietrabissa, A micro/nanoscale surface mechanical study on morpho-functional changes in multilineage-differentiated human mesenchymal stem cells, Macromol. Biosci. 7 (2007) 589–598. doi:10.1002/mabi.200600271.

[64] K.J.L. Burg, W.D. Holder, C.R. Culberson, R.J. Beiler, K.G. Greene, A.B. Loebsack, W.D. Roland, P. Eiselt, D.J. Mooney, C.R. Halberstadt, Comparative study of seeding methods for three-dimensional polymeric scaffolds, J. Biomed. Mater. Res. 51 (2000) 642–649. doi:10.1002/1097-4636(20000915)51:4<642::AID-JBM12>3.0.CO;2-L.

[65] H.J. Yoon, S.R. Shin, J.M. Cha, S.-H. Lee, J.T. Do, H. Song, H. Bae, Cold Water Fish Gelatin Methacryloyl Hydrogel for Tissue EngineeringApplication Hee, PLoS One. 11 (2016) e0163902. doi:10.1371/journal.pone.0163902.

[66] G. Yang, Z. Xiao, H. Long, K. Ma, J. Zhang, X. Ren, J. Zhang, Assessment of the characteristics and biocompatibility of gelatin sponge scaffolds prepared by various crosslinking methods, Sci. Rep. 8 (2018) 1–13. doi:10.1038/s41598-018-20006-y.

[67] A. Bouloumié, C. Sengenès, G. Portolan, J. Galitzky, M. Lafontan, Adipocyte Produces Matrix Metalloproteinases 2 and 9 Involvement in Adipose Differentiation, Diabetes. 50 (2001) 2080–2086. doi:10.2337/diabetes.50.9.2080.

[68] C. Vyas, R. Pereira, B. Huang, F. Liu, W. Wang, P. Bartolo, Engineering the vasculature with additive manufacturing, Curr. Opin. Biomed. Eng. 2 (2017) 1–13. doi:10.1016/j.cobme.2017.05.008.

[69] P. Datta, B. Ayan, I.T. Ozbolat, Bioprinting for vascular and vascularized tissue biofabrication, Acta Biomater. 51 (2017) 1–20. doi:10.1016/j.actbio.2017.01.035.

[70] Q. Zhang, J. Hubenak, T. Iyyanki, E. Alred, K.C. Turza, G. Davis, E.I. Chang, C.D. Branch-Brooks, E.K. Beahm, C.E. Butler, Engineering vascularized soft tissue flaps in an animal model using human adipose-derived stem cells and VEGF+PLGA/PEG microspheres on a collagen-chitosan scaffold with a flow-through vascular pedicle, Biomaterials. 73 (2015) 198–213. doi:10.1016/j.biomaterials.2015.09.024.

[71] L. Hutley, W. Shurety, F. Newell, R. McGeary, N. Pelton, J. Grant, A. Herington, D. Cameron, J. Whitehead, J. Prins, Fibroblast growth factor 1: A key regulator of human adipogenesis, Diabetes. 53 (2004) 3097–3106. doi:10.2337/diabetes.53.12.3097.

[72] M.L. Moya, M.H. Cheng, J.J. Huang, M.E. Francis-Sedlak, S. wei Kao, E.C. Opara, E.M. Brey, The effect of FGF-1 loaded alginate microbeads on neovascularization and adipogenesis in a vascular pedicle model of adipose tissue engineering, Biomaterials. 31 (2010) 2816–2826. doi:10.1016/j.biomaterials.2009.12.053.

[73] J. Michael Sorrell, M.A. Baber, D.O. Traktuev, K.L. March, A.I. Caplan, The creation of an in vitro adipose tissue that contains a vascular-adipocyte complex, Biomaterials. 32 (2011) 9667–9676. doi:10.1016/j.biomaterials.2011.08.090.

[74] J.H. Kang, J.M. Gimble, D.L. Kaplan, In Vitro 3D Model for Human Vascularized Adipose Tissue, Tissue Eng. Part A. 15 (2009) 2227–2236. doi:10.1089/ten.tea.2008.0469.

[75] M.P. Chhaya, F.P.W. Melchels, B.M. Holzapfel, J.G. Baldwin, D.W. Hutmacher, Sustained regeneration of high-volume adipose tissue for breast reconstruction using computer aided design and biomanufacturing, Biomaterials. 52 (2015) 551–560. doi:10.1016/j.biomaterials.2015.01.025.

[76] R. Sooppan, S.J. Paulsen, J. Han, A.H. Ta, P. Dinh, A.C. Gaffey, C. Venkataraman, A. Trubelja, G. Hung, J.S. Miller, P. Atluri, *In Vivo* Anastomosis and Perfusion of a Three-Dimensionally-Printed Construct Containing Microchannel Networks, Tissue Eng. Part C Methods. 22 (2016) 1–7. doi:10.1089/ten.tec.2015.0239.

[77] S. Kress, J. Baur, C. Otto, N. Burkard, J. Braspenning, H. Walles, J. Nickel, M. Metzger, Evaluation of a Miniaturized Biologically Vascularized Scaffold in vitro and in vivo, Sci. Rep. 8 (2018) 1–13. doi:10.1038/s41598-018-22688-w.

[78] N. Celikkin, J.S. Padial, M. Costantini, H. Hendrikse, R. Cohn, C.J. Wilson, A.E. Rowan, W.

Święszkowski, 3D printing of thermoresponsive polyisocyanide (PIC) hydrogels as bioink and fugitive material for tissue engineering, Polymers (Basel). 10 (2018). doi:10.3390/polym10050555.

[79] A.P. Golden, J. Tien, Fabrication of microfluidic hydrogels using molded gelatin as a sacrificial element, Lab Chip. 7 (2007) 720. doi:10.1039/b618409j.

[80] L.M. Bellan, S.P. Singh, P.W. Henderson, T.J. Porri, H.G. Craighead, J.A. Spector, Fabrication of an artificial 3-dimensional vascular network using sacrificial sugar structures, Soft Matter. 5 (2009) 1354. doi:10.1039/b819905a.

[81] X.-Y. Wang, Z.-H. Jin, B.-W. Gan, S.-W. Lv, M. Xie, W.-H. Huang, Engineering interconnected 3D vascular networks in hydrogels using molded sodium alginate lattice as the sacrificial template, Lab Chip. 14 (2014) 2709–2716. doi:10.1039/C4LC00069B.

[82] K. Li, Y. Xu, Citrate metabolism in blood transfusions and its relationship due to metabolic alkalosis and respiratory acidosis, Int. J. Clin. Exp. Med. 8 (2015) 6578–6584.

[83] H. Gong, J. Agustin, D. Wootton, J.G. Zhou, Biomimetic design and fabrication of porous chitosan-gelatin liver scaffolds with hierarchical channel network, J. Mater. Sci. Mater. Med. 25 (2014) 113–120. doi:10.1007/s10856-013-5061-8.

[84] A.W. Justin, R.A. Brooks, A.E. Markaki, Multi-Casting Approach for Vascular Networks in Cellularized Hydrogels Multi-Casting Approach for Vascular Networks in Cellularized Hydrogels, J. R. Soc. Interface. 13 (2016).

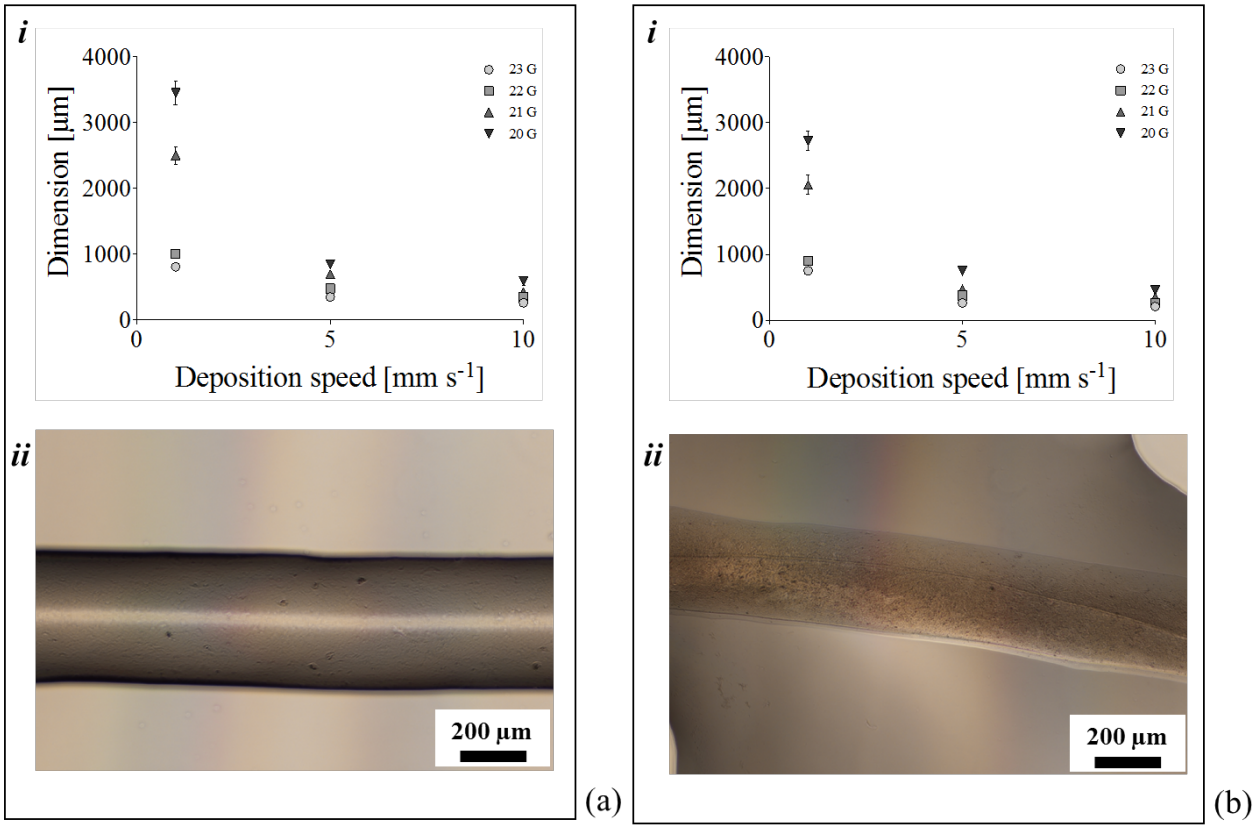


**Supplementary Information - Figure S1.** Alginate hydrogel 3D printing optimization (applied pressure fixed at 20 kPa) varying needle size and deposition speed. Average diameter of deposited 10% w/v alginate solution (a) before and (b) after crosslinking in 100 mM $CaCl_2$ solution (n = 3 measurements on n = 4 images per tested condition; data are expressed as N ± SD.).

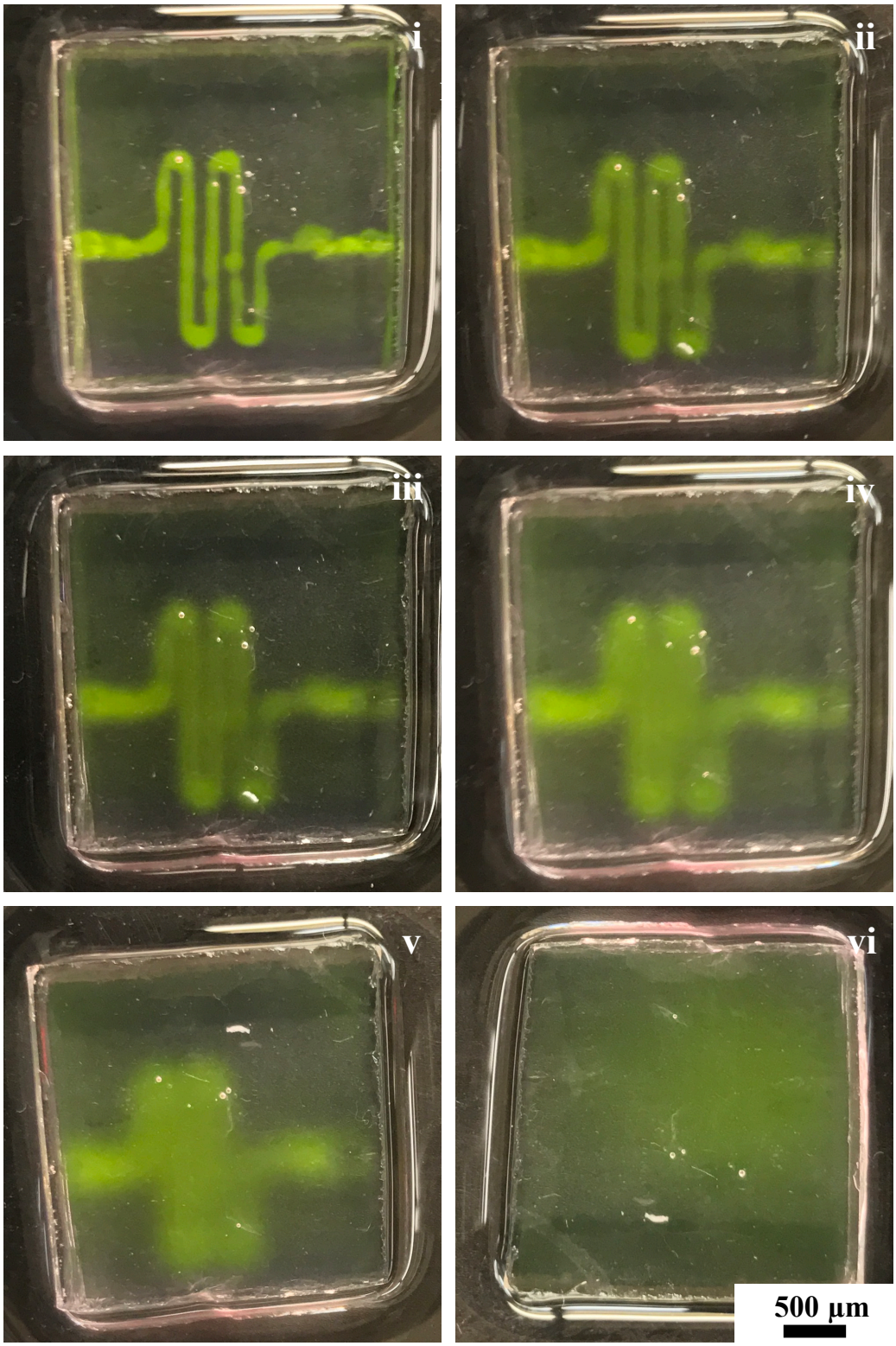


**Supplementary Information - Figure S2.** Qualitative diffusion of Rhodamine-6G in gelatin hydrogels. After 3D printed alginate dissolution inside the gelatin hydrogels to obtain a hollow channel, Rhodamine-6G solution (*i*) was injected in the channels and macroscopic images were taken after (*ii*) 20 min, (*iii*) 40 min, (*iv*) 1 h, (*v*) 2 h and (*vi*) 1 day.

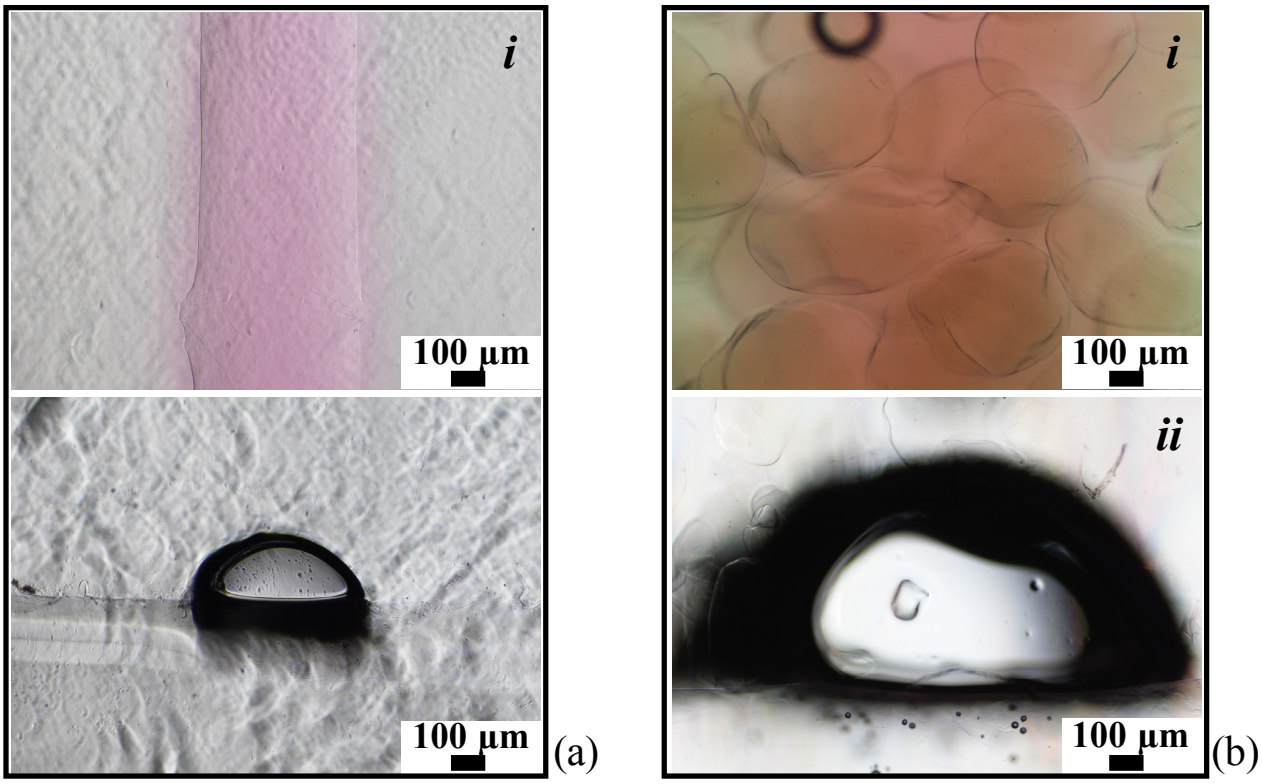


**Supplementary Information - Figure S3.** Representative images of (*i*) top view and (*ii*) section of hollow channels obtained after 3D printed alginate hydrogel selective removal in (a) gelatin hydrogels and (b) porous gelatin hydrogels. The different dimensions of the channels were obtained by varying the 3D printing parameters. In the gelatin hydrogels (a) the channels were produced with the lowest dimension that allowed the manual connections with the needles; in the gelatin hydrogels (b) the channels were produced with bigger dimension to allow an easier handling of the porous material.

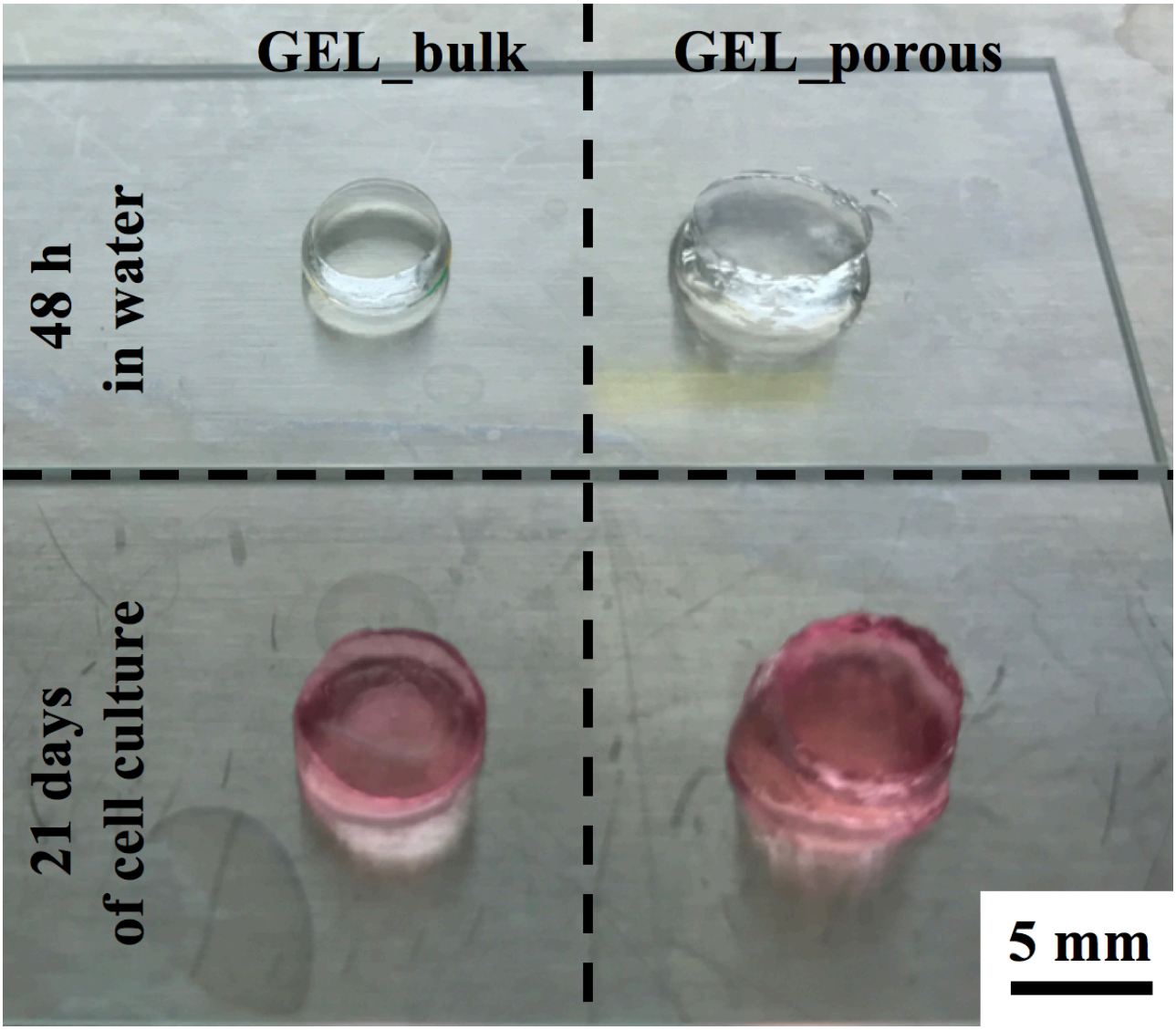


**Supplementary Information - Figure S4.** Macroscopic appearance of GEL_bulk (left column) and GEL_porous (right column) after 48 h of swelling in distilled water (0.02% w/v sodium azide, upper row) and after 21 days of hMSC culture (lower row).

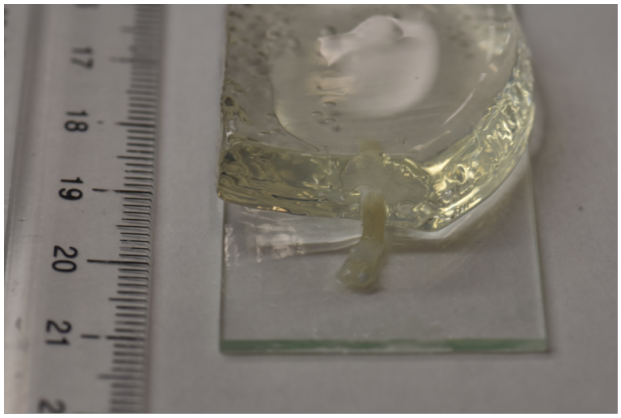

(a)
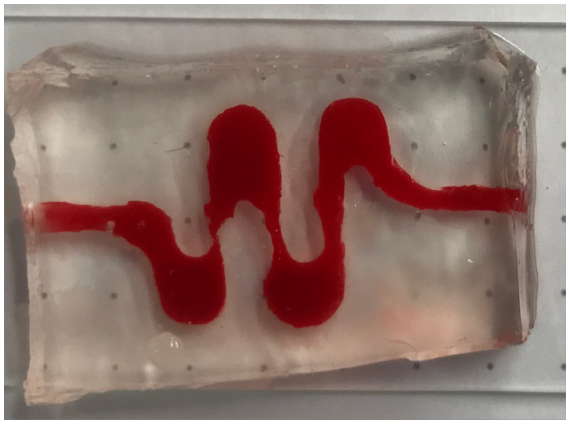
(b)

**Supplementary Information - Figure S5.** *Ex vivo* blood flow tests. Representative image of rat blood vessel inserted in the gelatin hydrogels hollow channels as inlet channel to be connected to the organism arteriosus system. (b) Representative image of pig blood flown inside the vascularizable gelatin hydrogels channels.